Master's Thesis

Thermal Measurement and Thermal Modelling of Electrical Insulation Systems in Electric Machines

REPORT

Author: Mohammad Roozbahani
Director: Eugenio Schillaci
Supervisor: Anders Thibblin
Call: June 2022

Escola Tècnica Superior

d'Enginyeria Industrial de Barcelona

Abstract

Thermal Measurement and Thermal Modelling of Electrical Insulation Systems in Electric Machines

Improved cooling in electric machines is of importance to achieve enhanced performance in electric machines and, in general, a necessary step in Scania's transition to electrification. The cooling of electric machines can be improved in several aspects, and one crucial part is to improve the thermal conductivity of insulating materials within stator slots. The majority of thermal conductivity resistance in the stator, which opposes heat extraction, is due to the electrical insulation materials used inside the slots. In this thesis project, several GPMs, made with different combinations of insulating materials have gone through thermal measurements in order to compare their thermal conductivity. Afterwards, the effect of thermal aging has been investigated on the thermal conductivity of insulating materials using accelerated aging methods. Furthermore, a 2D model has been developed in COMSOL and MATLAB to evaluate the equivalent thermal conductivity of each insulation layer combination.

The report starts with a short description of the electric machines' cooling mechanisms and heat generation sources. Basic theoretical knowledge in heat transfer that is required during the project is presented. This project explains the steps and challenges of manufacturing GPMs in the lab environment and all the errors and difficulties experienced during the experimental thermal measurement. Finally, validation of simulations using experimental data and utilizing these models to measure the effective thermal conductivity of materials is explained. Further investigation of experimental observation is continued by cutting GPMs and performing SEM (Scanning electron microscope) analysis. Finally, the report concludes by demonstrating the equivalent thermal conductivity of electrical insulation material together with their pros and cons.

Nomenclature

Abbreviations

GPM	General Purpose Model
PMSM	Permanent Magnet Synchronous Motor
HTC	Heat Transfer Coefficient
EM	Electric Motor
EDS	Energy-dispersive X-ray Spectroscopy
PD	Partial Discharge
SEM	Scanning Electron Microscope

Symbols

K, λ	Thermal conductivity
Nu	Nusselt number
L	Characteristic length
T	Temperature
$C,\ n,\ K$	Constants obtained experimentally
Pr	Prandtl number
Gr	Grashof number
μ	Dynamic viscosity
β	Thermal expansion coefficient
ρ	Density
Cp	Isobaric Heat capacity
T_w	Wall temperature
T_{ext}	Air temperature
R	Thermal resistance
$\dot{Q}$	Heat flux
α	Convection heat transfer coefficient
Ra	Rayleigh number
N	Number of nodes in x direction
M	Number of nodes in y direction
Δx	Mesh size in x direction
Δy	Mesh size in y direction
$\dot{Q}_g$	Heat generation rate
u	Internal energy
K_{eq}	Equivalent thermal conductivity
V_p	Volume of the node
d	Distance between the nodes

Table of Contents

List of Figures

List of Tables

Short Description of the Company

Scania AB is a major Swedish manufacturer headquartered in Södertälje, focusing on commercial vehicles—specifically heavy lorries, trucks and buses. It also manufactures diesel engines for heavy vehicles as well as marine and general industrial applications.

Scania is now undergoing a transformation from being a supplier of trucks, buses and engines to a supplier of complete and sustainable transport solutions. Electrified vehicles are one large part of that transformation.

This thesis project has been performed in YTME within Scania. The main focus of YTME or material technologies for electrification is on the parts such as electric machines, batteries, manufacturing quality of electric components, and power electronics involved in electric vehicles.

1. Introduction

1.1. Context of the Work

By growing the share of renewable energies and considering the targets set for zero-emission transportation by European countries, transportation companies now are focused on the electrification of their products more than any time in the past. As one of the world-leading companies in transportation, Scania is going through the same changes. According to Scania's electrification road map, by 2030, more than 50 percent of its products should be electrified [1] and Scania is committed to being fully net-zero by 2040 [2]. With the electrification of transportation, the demand for efficient, high power/torque density and compact electric motors is also increasing [3]. One limiting aspect for the optimal performance of electric machines is their ability to dissipate the generated heat. Increasing the torque density typically requires high electrical loading in the armature windings. Moreover, the peak current required in the acceleration of an EV generates a huge amount of heat in a short time. If the generated heat is not removed properly, excessive heating will degrade the windings and insulation material's life and will damage the motor with time [4].

In recent years, several passive and active strategies and methods have been investigated to improve the cooling of electric machines [5]. The most efficient way of heat removal is to cool the electric motor using the circulation of intermediary fluids like air, water, or oil. However, the heat generated by the electric and magnetic losses has to be transferred through solid materials like insulation layer, slot liner, stator etc., before reaching the cooling fluid.

In order to obtain electric machines with high efficiency, high power density and high reliability, materials with improved thermal conductivity are of importance. The properties of the materials in the electrical insulation system can be evaluated by using General Purpose Models (GPM), which are small segments of the stator ring. By using GPMs instead of full-size stators, many more material combinations can be explored.

This thesis project is particularly focused on improving the thermal conductivity of insulation materials in electric machines. The majority of the thermal conductivity resistance between the wires, which are the source of heat generation, and the stator surface is due to the electrical insulation material. The challenging part of this thesis project is that the insulation material should be a good conductor of heat and a good insulator of electric current at the same time. This fact greatly narrows the choice of material for this application. In parallel with this thesis project, another project is defined to investigate the electrical characteristics of the insulation material.

1.2. Thesis Objectives and Questions

Following questions describe the main targets of this thesis project and they should be answered at the end of the thesis:

1. How to assemble the test setup?
    a. How to improve the design of GPMs?
    b. How to increase the accuracy of the measurements?
    c. How to decrease the number of experiments?
2. Which combination of wire insulation, slot liner, and impregnation will lead to the optimal thermal performance?
3. How to develop an accurate simulation for the heat transfer in GPM and how to validate and put this model into use?
4. What will be the effect of thermal aging on the thermal conductivity of materials?

These are the main questions that during this Master's thesis we will try answer and propose solutions for them.

2. Literature Review

Thermal analysis of electric machines is generally more complex and challenging compared to the electromagnetic analysis in terms of developing the model and accuracy of the results. This is because of the fact that thermal behavior is highly dependent on the manufacturing qualities [6].

Thermal design engineering has become very important to develop smaller and more efficient electric motors, therefore electrical machine designers need to be more informed with the recent development in novel thermo-conductive (insulation) materials [7]. Figure 1 shows the importance of improving thermal conductivity of electrical materials, as one of the main development areas in U.S. Drive Electrical and Electronics Technical Team Roadmap.

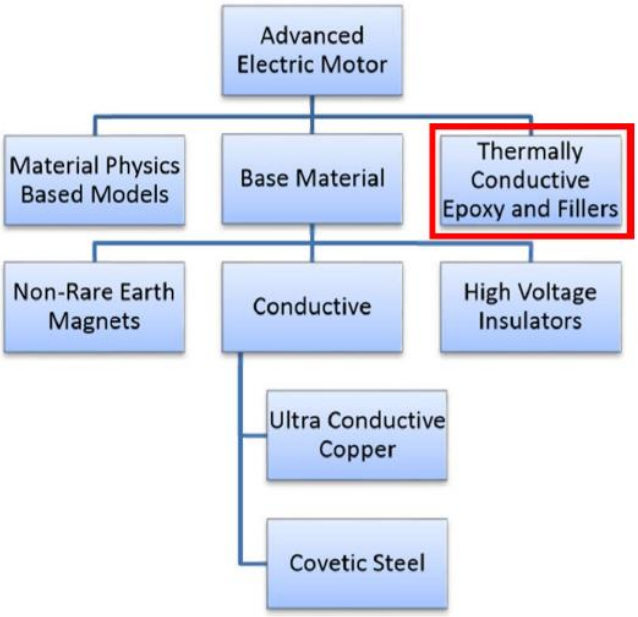

FIGURE 2. Electric motor research and development (R&D) areas according to U.S. Drive Electrical and Electronics Technical Team Roadmap [26].

Figure 1. Electric motor research and development areas according U.S. Drive Electrical and Electronics Technical Team Roadmap [7]

Thermal conductivity of different insulating material can be measured separately using one dimensional Fourier law of heat transfer as shown in Figure 2 [8].

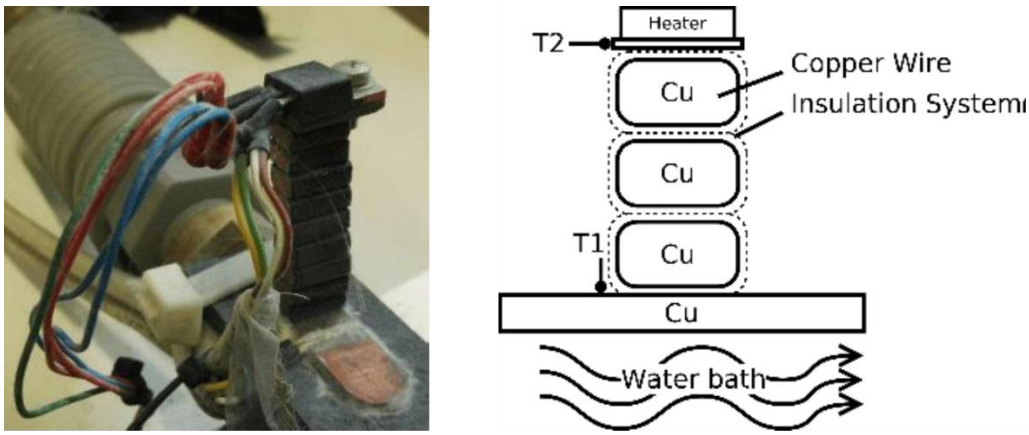

Figure 2. (a) A segment of winding to measure thermal conductivity, (b) the principle of direct thermal conductivity measurement [8]

2.1. Electric Machines

Electric machines are devices that convert electrical work to mechanical and vice versa. These machines use electromagnetic force to convert mechanical and electrical power. Machines that convert mechanical power to electrical are called generators, and the ones that convert electrical power to mechanical are called electric motors. Each category can also be divided into two general groups based on their operation principles, i.e. synchronous and asynchronous machines. The focus of this report is on Permanent Magnet Synchronous Motor (PMSM) which is the type of motor that Scania is using and also one of the widely used motors in electric vehicles.

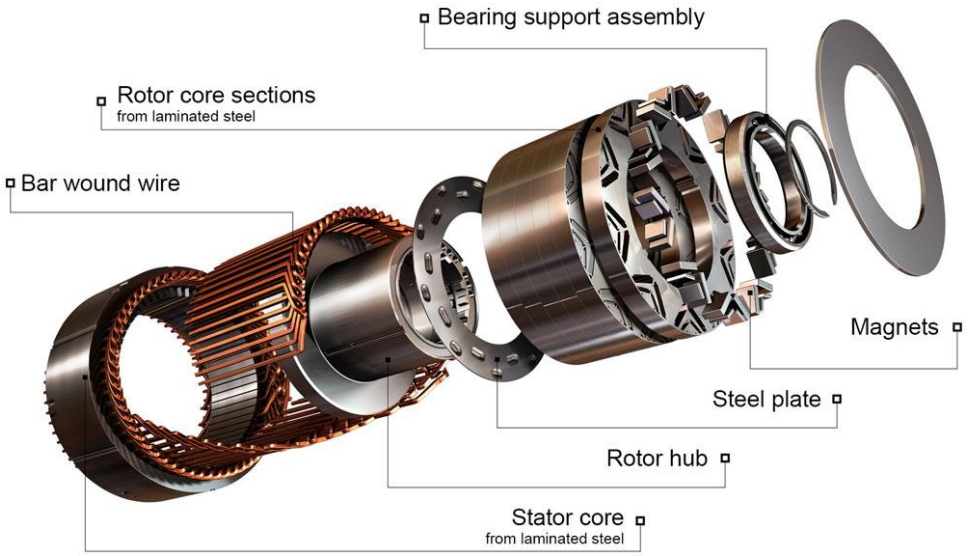

Figure 3. PMSM configuration and components [9]

2.2. Heat generation sources in EM

There are several types of heat generation sources in a working EM. Heat generation is caused by varying magnetic and electric fields, mechanical losses, and joule heating in electrical wires. In machine terminology, these heat sources are commonly referred to as losses since they arise as a difference between input power and output power in the conversion process [10]. So the three heat generation sources in electric machines can be categorized as:

- Magnetic losses
- Electric losses
- Mechanical losses

It has been observed in the previous thesis work at Scania [11] that the most effective approach for heating the coils inside the stator is Joule heating. Out of the three heat generation sources mentioned, electrical losses contribute the most to the heating of electric machines. In the real case, the ratio of iron loss to copper loss is 3.62% under the rated current [12]. So, the assumption that heat generation is happening just in the copper wires is reasonable.

Understanding and predicting temperature evolution in an electric motor using heat transfer models and employing the results to make better design decisions is critical to avoid motor failure.

2.3. Effect of insulation aging on heat transfer

During an electrical machine's lifetime, it will go through numerous thermal, electrical, and vibrational stress cycle that will greatly affect the properties of insulation material used in the motor during the time.

Insulation materials typically used in electric machines show a degradation in their insulating properties when exposed to elevated temperatures. Degraded insulation performance renders a higher risk for short-circuits and potential catastrophic failure of the machine. Thermal stress can be a result of stresses like: thermal, vibration, humidity, and electrical [3]. However, the focus in this project is on thermal aging. To be able to observe the effect of thermal aging on the properties of insulation material for the different combination in the limited time of this thesis, accelerated aging technique has been employed.

[13] proposed the following equation which is based on a chemistry approach to estimate the insulation aging in electric machines:

$$L = Ae^{-\frac{B}{T}}$$

Where:

$$L: life$$

$$A \ \& \ B: constants$$

$$T: absolute\ temperature$$

3. Theory

3.1. Basics of Conduction Heat Transfer

In general there are three main heat transfer mechanisms: conduction, convection, and radiation. Radiation heat transfer will be considered mainly in a high temperature applications (>1000 K) [14]. Hence, in this case the major heat transfer mechanisms that are involved in the cooling of the EM are conduction and convection. The main focus of this thesis is particularly on the improvement of the heat conduction from the electrical wires to the surface of the stator. Oil is the fluid that is used for removing the heat from the stator using forced convection but this topic is out of this thesis scope.

Heat conduction phenomena is governed by the Fourier's law. This equation states that the rate of heat transfer is proportional to the gradient of temperature in the materials.

$$\dot{Q} = -k\nabla T \tag{1}$$

Where k is the thermal conductivity (W/m/K) of the solid medium, T is the temperature, and q is the conduction heat transfer.

3.2. Convection heat transfer

The external flow by natural convection for the horizontal plate is fairly simple to solve for. We know that the external fluid is ambient air. We essentially need to find the external heat transfer coefficient, α_{ext}, which we can then later use in the discretization analysis to determine the evolution of wall temperature for the stator. The external heat transfer coefficient depends on Nusselt number, which depends on whether the flow is laminar or turbulent, and also on the Rayleigh number. The Rayleigh number depends on the Prandtl number, and the Reynolds number.

To calculate the average heat transfer coefficient at the outside surface, we need to calculate some thermophysical properties. The empirical equations for calculating thermophysical properties are taken from [15]. Thermodynamical properties should be calculated in the film temperature. Film temperature is the average of wall and ambient temperatures. The ambient temperature is 21°C and the wall temperature is assumed to be 70°C. Hence, the average temperature of the film temperature will be 45.5°C.

The thermal expansion coefficient β_{ext} is given as:

$$\beta = \frac{1}{T}\ for\ air \tag{2}$$

$$\beta_{ext} = \frac{1}{45.5 + 273.15} = 31 * 10^{-4}\frac{1}{K} \tag{3}$$

The thermal conductivity λ_{ext} is given as [15]:

$$\lambda_{ext} = \frac{2.648 * 10^{-3}\sqrt{T}}{1 + \left(\frac{245.4}{T}\right) * 10^{\frac{-12}{T}}} = 0.0277\ \frac{W}{mK} \tag{4}$$

The viscosity is given as [15]:

$$\mu_{ext} = \frac{1.458 * 10^{-6}T^{1.5}}{T + 110.40} = 1.9329 * 10^{-5}\ \frac{kg}{ms} \tag{5}$$

The specific heat capacity is given as :

$$cp_{ext} = 1034.09 - 2.849 \cdot 10^{-1}\mathrm{T} + 7.817 \cdot 10^{-4}\mathrm{T}^2 - 4.971 \cdot 10^{-7}\mathrm{T}^3 + 1.077 \cdot 10^{-10}\mathrm{T}^4 \tag{6}$$

$$cp_{ext} = 1007.7\frac{J}{KgK} \tag{7}$$

The density is given by:

$$\rho_{ext} = f(P_{ext}, T_{ext}) \tag{8}$$

$$\rho_{ext} = \frac{P_{ext}}{287T_{ext}} = 1.108\frac{\mathrm{kg}}{m^3} \tag{9}$$

The Prandtl number is given as:

$$Pr_{ext} = \frac{\mu_{ext}cp_{ext}}{\lambda_{ext}} = 0.703 \tag{10}$$

The Grashof number is given as:

$$Gr_{ext} = \frac{g\beta\rho_{ext}^2|T_w - T_{ext}|L^3}{\mu_{ext}^2} \tag{11}$$

$$Gr_{ext} = \frac{g\beta\rho_{ext}^2|T_w - T_{ext}|L^3}{\mu_{ext}^2} = 23477 \tag{12}$$

The Rayleigh number is the product of Prandtl and Grashof number.

$$Ra_{ext} = Pr_{ext} * Gr_{ext} = 16506 \tag{13}$$

From empirical equations the Nusselt number for this case is given as:

$$Nu = CRa^nK \tag{14}$$

The flow is laminar flow:

$$C = 0.54, n = 0.25, K = 1$$

$$Nu_{ext} = 6.12$$

The convective heat transfer coefficient which will be used in the simulations, is given as:

$$\alpha = \frac{\lambda_{ext}\, Nu_{ext}}{L} = 10.09 \frac{W}{m^2 K} \tag{15}$$

3.3. Thermal contact resistance

One major resistance in heat extraction from the coils is the thermal contact resistance that exist in the connection point of solid materials. The thermal contact resistance is originated from surface roughness of materials which prevents from perfect thermal connection (Figure 4). Due to the surface roughness, gaps, which are most commonly are filled with air, will appear in connection area. Therefore, in the contact surface there are two parallel thermal resistances. One from the solid contact spots and other from the gaps [15].

$$R' = \frac{T_A - T_B}{q"} \tag{16}$$

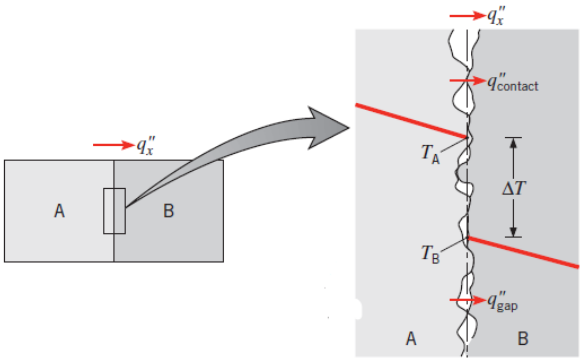

Figure 4. Thermal contact resistance between two solid materials [15]

In the solids that have a high thermal conductivity, the heat conduction can be increased by increasing the contact pressure and/or decreasing the surface roughness to minimize the gaps. Another approach that can decrease thermal contact resistance is to use fluids of high thermal conductivity as the filler of gaps [15].

Although there are several theories that have been developed for the calculation of thermal contact resistance, the most reliable results are the ones that have been obtained experimentally [15].

4. Methodology

This chapter will explain in detail the methodology that has been selected to approach the problem. It will start with introducing the test setup and the components used in the test. Materials used in the GPM and their related properties are presented. Later on, all the possible combinations of these materials used as the insulation layer are mentioned. Afterwards, the chapter addresses the pre-processing and processing of the models developed in MATLAB and COMSOL. And finally, the whole outline of the approach is explained.

The overall outline of the methodology can be divided into four major steps that needs to be taken. These four steps are:

- **Initial simulation**: Before finalizing the experiment setup, an initial simulation should be done to observe the temperature contour within GPMs. This simulation will help us to have a primary assessment of the experiments, despite being inaccurate. The assessment will indicate what range of temperature should be expected in the experiments and also suitable locations for thermocouples attachment can be selected.
- **Finalizing test setup**: After locating ideal locations to read the temperature, thermocouples were attached to the GPM using soldering. Hence, the GPMs were completed and they were ready for the measurements. The chosen locations should be both ideal and feasible to attach.
- **Performing experiments**: After attaching the thermocouples, the measurements will start and the GPMs will go through heating. The measurements will be repeated at least three times for each set of GPM to make sure the results are adequate.
- **Validating simulations**: The results obtained from the experiments will be used to validate the models. The parameters that need to be validated are heat generation, heat convection, and thermal conductivity of the insulating material. Later on, this model will be used for the comparison of the thermal conductivity in different GPMs.

4.1. Experimentation

4.1.1. GPM configuration

General Purpose Model (GPM) is a simplified version of actual electric machines for the purpose of performing experiments. The GPM used in this project includes just one slot. The scale of the GPM is smaller than an actual electric motor and can include one or several slot of an actual electric machine depending on the objective of measurements.

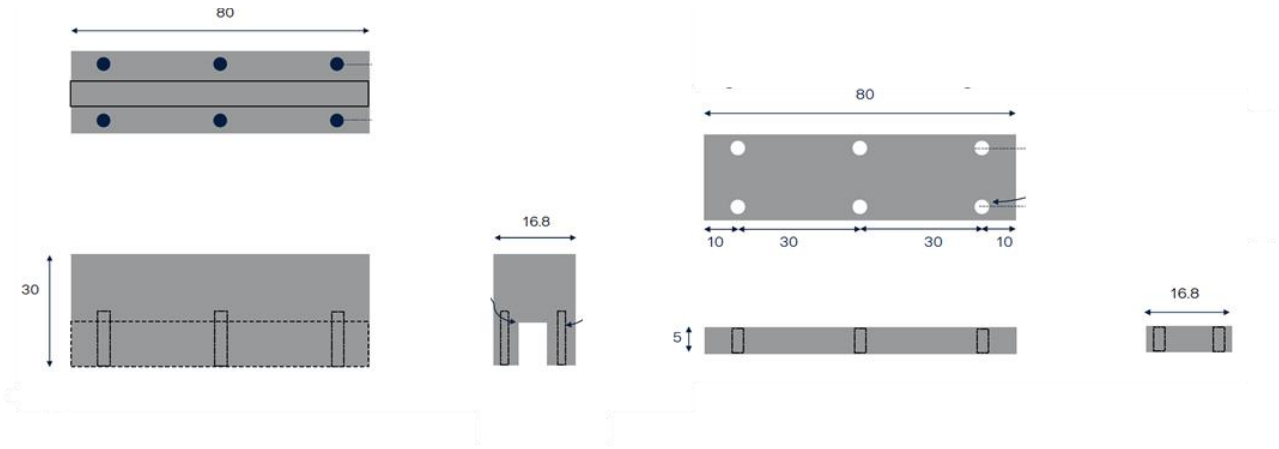

Figure 5. GPM configuration and outer dimensions

There are four wires inside the slot. These wires are separated from the stator steal with the slot liners to ensure that there is no electrical connection between the wires and stator. The remaining gaps in the slot are filled with the impregnation material to improve the overall thermal conductivity by replacing the gaps that are originally filled with the air. Figure 6 shows the order that wires, impregnation material, and slot liners are placed inside the stator slot in the GPMs. In the production phase, the resin (impregnation material) can penetrate into the gap between wires and also into the gap between slot liner and stator. For the production of GPMs, initially, the wires and slot liner are placed inside the slot. Afterwards, the impregnation that initially is in liquid state, first was pre-heated and then is injected to fill up the gaps and finally the whole setup is heated up to the curing temperature of the resin to solidify. After placing everything inside the slot and before solidification of the resin, an insulation plate (Figure 5, right) is screwed to keep everything inside the slot and prevent heat loss from the bottom.

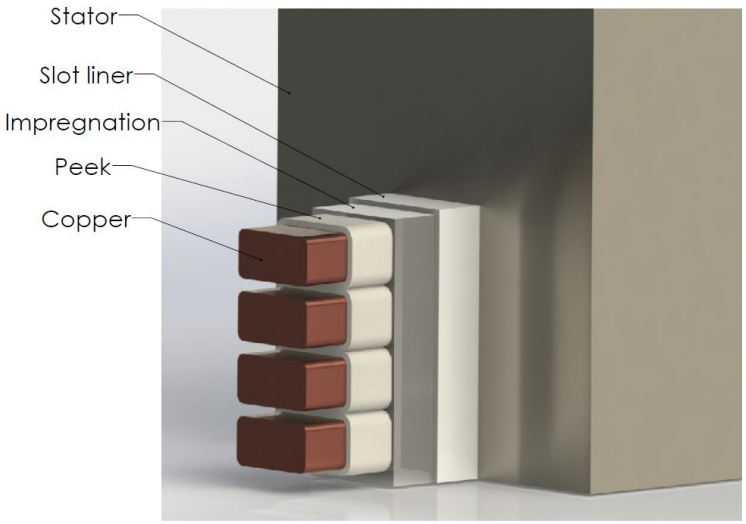

Figure 6. Demonstration of wires, impregnation, and slot liner inside the slot

Joule heating is the approach that has been chosen for the heating of wires. The wires are connected to a power source. The heat generation in the wires is controlled through adjusting the current passing through them using power source (Delta Elektronika SM 45 -70 D).

4.1.2. Material Properties

Table 1 shows all the materials used in this project together with their relevant thermophysical characteristics. Due to the confidentiality, the name of the impregnation will be addressed as R1 anD-R2 and the Slot liners will be addressed as A, B, C, D. Since our studies are focused on the thermal behavior of the GPM, the involved properties are thermal conductivity, heat capacity, and density of the materials used. Heat capacity and density which represent the thermal inertia, are associated with the transient nature of the simulations. In the steady-state condition, the thermal conductivity of the materials would be enough to solve the problem. The parameters in Table 1 are all extracted from the datasheet of materials that is provided by suppliers, and the data that wasn't accessible was approximated.

Part	Material	Thermal conductivity (W/m/K)
Stator	Steel SS2541	38 - 42.6*
Wire	Copper	413*
Wire insulation	PEEK	0.25
Impregnation	R1	0.22
	R2	0.5-0.6
Slot liner	A	0.22
	B	0.21
	C	0.3
	D	0.36

Table 1. Materials used in the GPM and their important characteristics, properties with * sign are approximated

Insulating materials in the slot refers to wire insulation, impregnation, and slot liner. In this thesis, there are four types of slot liners and two types of impregnation which presents us with a total of eight different possibilities for insulation. Since some thermal and electrical experiments can be destructive, two of each particular GPM was made that means a total of sixteen GPMs (eight pairs, Table 2). GPMs of the same kind are called GPM 1(a) and GPM 1(b). Also, GPM 8 was missing the pair due to the lack of stator segments.

Number	Slot liner	Impregnation	Name of the GPM
GPM 1	A	R1	A-R1
GPM 2	B	R1	B-R1
GPM 3	C	R1	C-R1
GPM 4	D	R1	D-R1
GPM 5	A	R2	A-R2
GPM 6	B	R2	B-R2
GPM 7	C	R2	C-R2
GPM 8	D	R2	D-R2

Table 2. Different composition for GPMs

4.1.3. Test Setup

After finishing the production of GPMs, they are now ready to go through thermal and also electrical tests. In order to model the actual thermal boundary conditions that a real stator segment will experience, the GPMs are embedded inside an insulation box which is 3D printed using a low thermal conductivity material (Ultem 1010) and with a honeycomb structure to further reduce the thermal conductivity (Figure 7). The purpose of using this insulation box is to have insulation in the sidewalls and the bottom of GPM as the actual segment does. Hence, the heat transfer is just allowed from the top surface of GPM through natural convection. The thermal insulation boundary condition in the real stator segment is due to the axial symmetry that exists in an EM (Figure 9). It also should be noticed that in the actual EM, the cooling is done using oil circulating and creating forced convection. However, this paper's objective is to compare insulating materials, and that can be done as long as the measurements have been performed under identical conditions for all the materials.

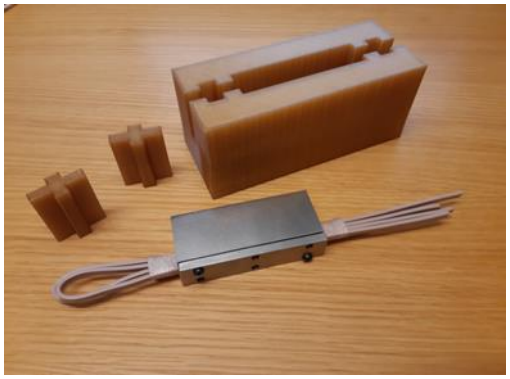

Figure 7. A completed GPM together with insulation box

Figure 8. Figures of thermocouple (a), data logger (b), and memory card (c)

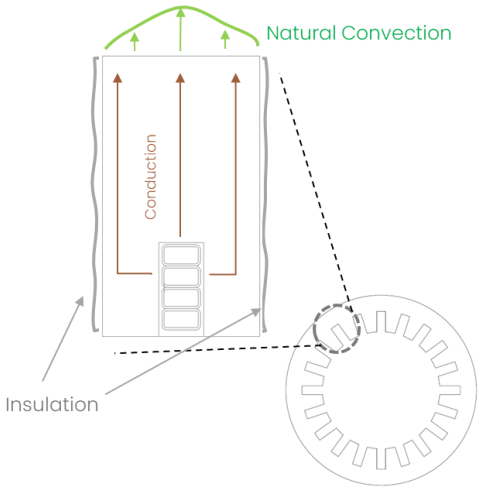

Figure 9. Thermal boundary conditions in stator segment

Parts of the experimental setup is shown in Figure 8 and a complete test setup is shown in Figure 10. The test setup includes a power source, thermocouples (type k), data logger (EXTECH), and the GPM embedded inside the insulation box. Since each GPM needed almost two hours to reach steady-state condition, each pair of GPMs was connected in series and heated up simultaneously to save time. Since the two GPMs are connected in series, the same current is passing through the wires inside them, which means equal heating values are expected for both GPMs. To be able to measure the thermal conductivity of the insulating material, the temperature on the wire and on the stator top surface is measured. Measurement of temperature on the wire requires the PEEK layer to be removed before connecting the thermocouples to the copper. That will have undesirable effects on electrical partial discharge (PD) experiments. Hence, just one of the GPMs from each type has the thermocouples on the wire. The temperature meter has four thermocouple inputs. Table 3 describes the parameter that each input is displaying.

Soldering has been used to attach the thermocouples to the stator surface and also to ensure an excellent thermal connection between thermocouples and the surface. For some connections, especially on wire surfaces, in which attaching thermocouples using soldering was difficult, glue was used for attachment. The power source is set on 60A. Each set of GPMs had a different value of resistance which depends on the connections between wires. So to ensure that the current is set on 60A, voltage values had to vary between 1V to 1.5V for different GPM sets.

To reach steady-state condition in each experiment, between two to three hours was required depending on how well the GPM is placed inside the insulation box. However, since the main objective of the test was to compare insulating material and the transient behavior was more important to us, it was decided to truncate the measurement after 1.5 hours. Transient behavior is important because in an actual electric machine under real operating conditions, is unlikely to reaching a steady-state condition. Moreover, to be able to validate the model and calculate the thermal conductivity, it is not necessary to reach steady-state.

Input number	Measured Parameter
T_1	Temperature of the wire in the GPM 1 (attached to the exposed wire)
T_2	Stator surface temperature in GPM 1
T_3	Stator surface temperature in GPM 2
T_4	Ambient temperature

Table 3. Data logger inputs (the parameters that each thermocouple is measuring)

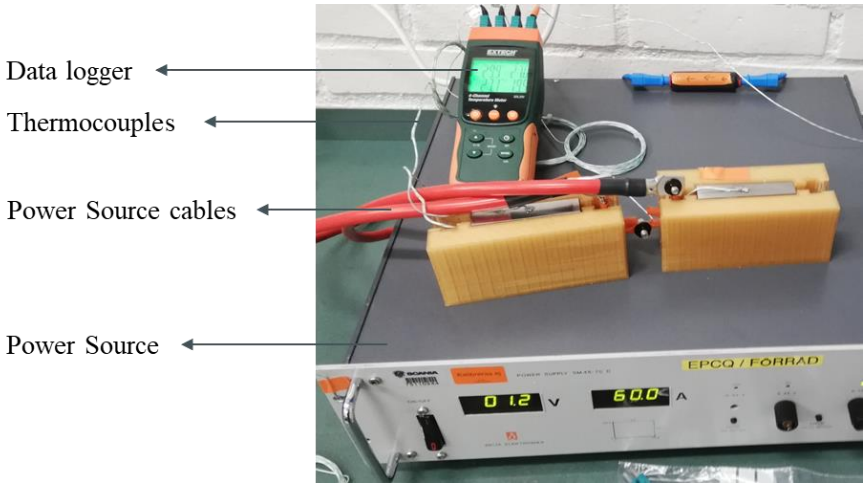

Figure 10. A complete test setup ready for temperature measurement

4.2. Simulation

4.2.1. COMSOL Model

COMSOL has been used for the initial thermal simulation of the GPM. The objective of this simulation was to observe an approximate temperature profile development in GPM's cross section to find the most effective and feasible locations for implementing thermocouples in the real test setup.

Considering the number of simulations, it was decided to perform the simulation in 2D planar to simplify the model and avoid huge computational efforts. Hence, the geometry of the model is the cross-section of the GPM (Figure 11). The only physics that was required for this simulation was the "heat transfer in solids" module in COMSOL. There are two options for modelling the heat convection around the GPM. First option in two solve the Navier-Stokes equations for the air flow around the GPM. The advantage of this method is that the air flow behavior around the GPM can be visualized. However, since we need to solve Navier-Stokes equations, this method requires a huge amount of computational effort. In the second method, the convection heat transfer in GPM is calculated using a constant heat transfer coefficient (HTC) calculated from empirical relations. Using this method will decrease the simulation time drastically but

we have no information about the air flow around the GPM. Since in the scope of this Master's thesis, the focus is on thermal conductivity of insulation material and the air behavior around the GPM is of no interest, constant convection HTC method has been used. The calculation of the natural convection HTC has been done in section 3.2.

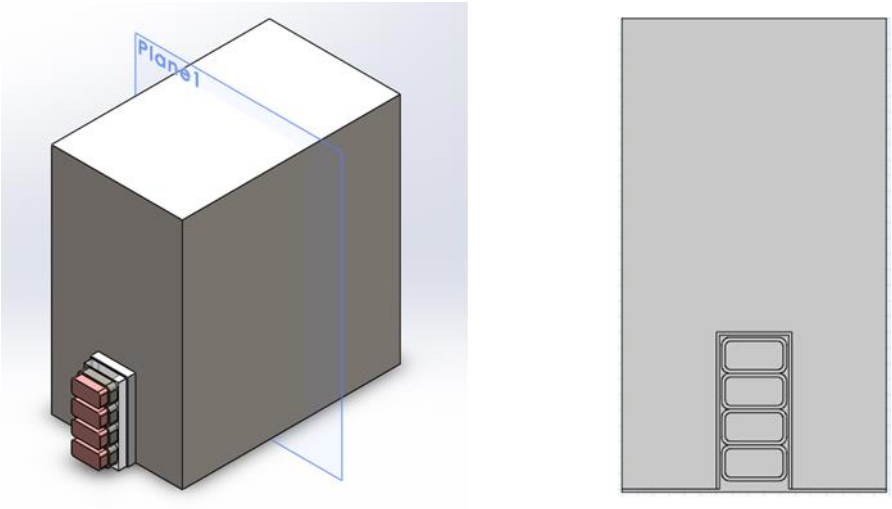

Figure 11. Cross section of the GPM

The 2D geometry was developed and imported to COMSOL from AutoCAD. As explained previously in section 4.1.3 the transient state is important to us so the simulation is transient. The initial thermal boundary conditions and mesh of the model are demonstrated in Figure 12. Meshing has been generated using physics-controlled automatic mesh in COMSOL. The mesh density is higher around the slot to capture the high temperature gradients. The heat source in the GPM is the heat generated by Joule effect in the wires. Joule effect is modelled using a volumetric heat generation within the wires.

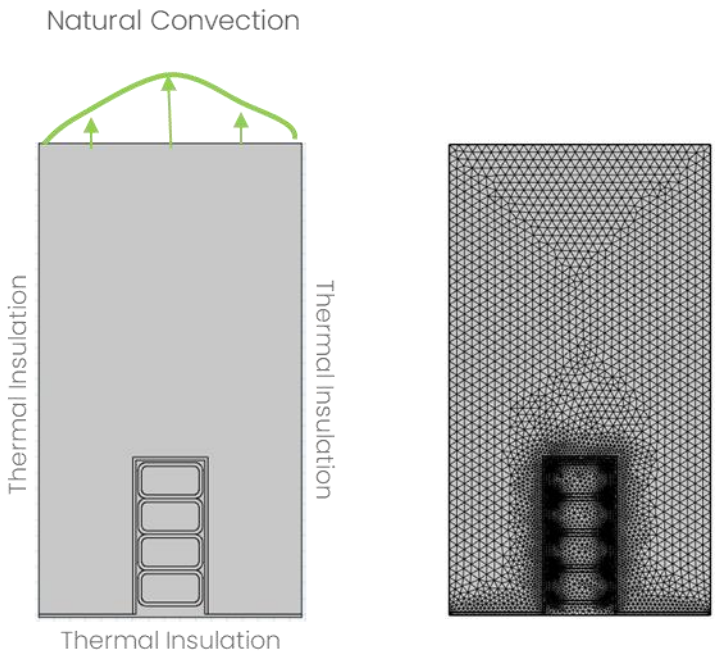

Figure 12. 2D geometry and the mesh in COMSOL

The material properties of interest that will be used in the simulations are thermal conductivity, heat capacity, and density. Since all the materials mentioned in Table 1 were not available in COMSOL library, they were added manually.

4.2.2. MATLAB Numerical Model

In order to explore other simulation possibilities and also to develop an original simulation methodology which will not be dependent on the availability of the commercial software, a code was developed to solve the transient 2D conduction heat transfer in MATLAB. Finite volume method (FVM) has been used for evaluating partial differential equations. The thermal boundary conditions are the same as explained in the previous section.

The first step is to apply the finite volume method. We take the wall and divide it into **N** control volumes in x direction and **M** control volumes in y direction. To avoid complexities in the code, a structured mesh has been used (Figure 13). However, the distribution of the nodes is not uniform in x and y direction and the nodes are distributed in a way that the density of the mesh is higher within stator slot. The discretization nodes are placed in the center of each control volume, and two additional nodes are placed on both the surfaces of the walls on the left and right ends. And so, in total, there are **(N+2)***(**M+2)** nodes. Each control volume has a surface equal to $\Delta x \times \Delta y$, which is given by:

$$\Delta x = \frac{L}{N} \tag{17}$$

$$\Delta y = \frac{H}{M} \tag{18}$$

Which L and H are the length of GPM's cross section in x and y directions respectively.

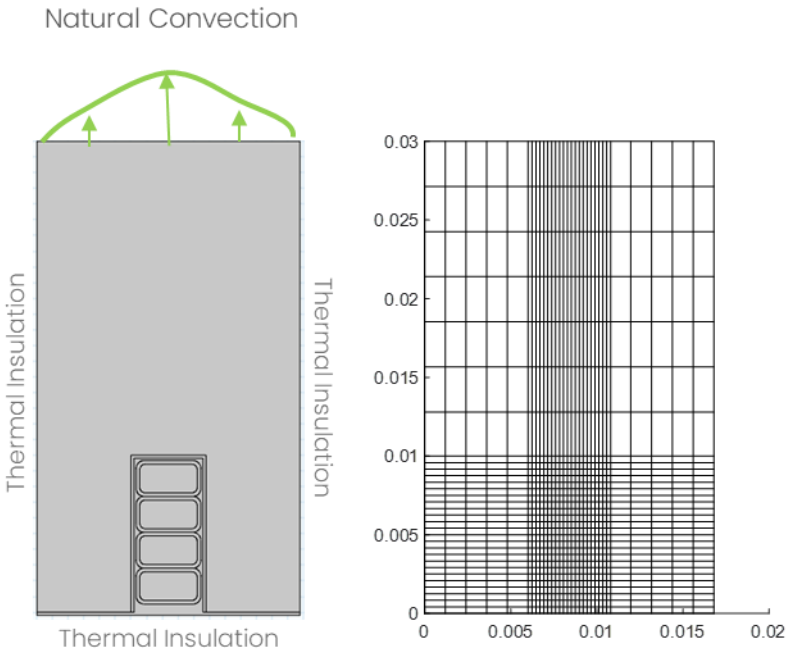

Figure 13. 2D geometry and the mesh MATLAB

The next step is to find discretization equations for all the nodes. Considering first the **internal nodes**, we can consider the heat transfer by the diagram below:

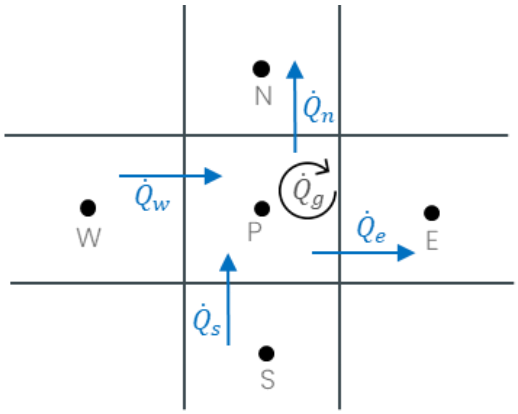

Figure 14. Conduction heat transfer from the adjacent nodes

Now, we know that from the total energy balance:

$$\frac{\partial}{\partial t}\int_{V_p} u\rho dt = \sum \dot{Q}_p \tag{19}$$

where $\sum \dot{Q}_p$ is the accumulation term, given by:

$$\sum \dot{Q}_p = \dot{Q}_w - \dot{Q}_e + \dot{Q}_s - \dot{Q}_n + \dot{Q}_{generation} \tag{20}$$

Knowing that density is constant as thermophysical properties have been assumed constant, and we know by definition that:

$$\overline{u_p} = \frac{1}{V_p}\int_{V_p} u dV \tag{21}$$

So,

$$\rho_P \frac{\partial \overline{u_p}}{\partial t} V_p = \sum \dot{Q}_p \tag{22}$$

Now integrating both sides with respect to time:

$$\int_{t^n}^{t^{n+1}} \rho_P V_p \frac{\partial \overline{u_p}}{\partial t} dt = \int_{t^n}^{t^{n+1}} \sum \dot{Q}_p \, dt \tag{23}$$

$$\rho_P V_p \left(\overline{u_p}^{n+1} - \overline{u_p}^{n}\right) = \int_{t^n}^{t^{n+1}} \sum \dot{Q}_p \, dt \tag{24}$$

$$\approx \rho_P V_p \left(u_p^{n+1} - u_p^{n}\right) = \int_{t^n}^{t^{n+1}} \sum \dot{Q}_p \, dt \tag{25}$$

Knowing that $du = c_p dT$,

$$\rho_P V_p c_p \left(T_p^{n+1} - T_p^{n}\right) = \int_{t^n}^{t^{n+1}} \sum \dot{Q}_p \, dt \tag{26}$$

The latter term of the equation depends on what time-integration scheme is implemented. We use the term β to choose between these integration schemes. So, our equation becomes:

$$\rho_P V_p c_p \left(T_p^{n+1} - T_p^{n}\right) = \left(\beta \sum \dot{Q}_p^{n+1} + (1-\beta) \sum \dot{Q}_p^{n}\right) \Delta t \tag{27}$$

Now it should be noted that for various time-integration schemes:

- Implicit → $\beta = 1$
- Explicit → $\beta = 0$
- Crank-Nicolson → $\beta = 0.5$

For the current case, we use the implicit case, because it is more stable than explicit. So, our equation becomes:

$$\rho_P V_p c_p\left(T_p^{n+1} - T_p^n\right) = \Delta t \sum \dot{Q}_p^{n+1} \tag{28}$$

$$\frac{\rho_P V_p c_p\left(T_p^{n+1} - T_p^n\right)}{\Delta t} = \sum \dot{Q}_p^{n+1} \tag{29}$$

We identified earlier that $\sum \dot{Q}_p = \dot{Q}_w - \dot{Q}_e + \dot{Q}_s - \dot{Q}_n$, and so:

$$\frac{\rho_P V_p c_p\left(T_p^{n+1} - T_p^n\right)}{\Delta t} = \dot{Q}_w^{n+1} - \dot{Q}_e^{n+1} + \dot{Q}_s^{n+1} - \dot{Q}_n^{n+1} + q_v.V_p \tag{30}$$

Now, we know that heat conduction is given as follows:

$$\dot{Q} = -\lambda \frac{dT}{dx} S \tag{31}$$

So:

$$\frac{\rho_P V_p c_p\left(T_p^{n+1} - T_p^n\right)}{\Delta t} = -\lambda_w \left.\frac{dT}{dx}\right|_w S_w + \lambda_e \left.\frac{dT}{dx}\right|_e S_e - \lambda_s \left.\frac{dT}{dx}\right|_s S_s + \lambda_n \left.\frac{dT}{dx}\right|_n S_n + q_v.V_p \tag{32}$$

$$\frac{\rho_P V_p c_p\left(T_p^{n+1} - T_p^n\right)}{\Delta t} = -\lambda_w \frac{T_p^{n+1} - T_w^{n+1}}{d_{pw}} S_w + \lambda_e \frac{T_e^{n+1} - T_p^{n+1}}{d_{pe}} S_e - \lambda_s \frac{T_p^{n+1} - T_s^{n+1}}{d_{ps}} S_s + \lambda_n \frac{T_n^{n+1} - T_p^{n+1}}{d_{pn}} S_n + q_v.V_p \tag{33}$$

Now we need to convert the equation in a form that we can find the discretization coefficients, which is the following form:

$$a_p T_p^{n+1} = a_e T_e^{n+1} + a_w T_w^{n+1} + a_n T_n^{n+1} + a_s T_s^{n+1} + b_p \tag{34}$$

So, our equation becomes:

$$\left[\frac{\rho_P V_p c_p}{\Delta t} + \frac{\lambda_e S_e}{d_{pe}} + \frac{\lambda_w S_w}{d_{pw}}\right]\left(T_p^{n+1}\right) = \frac{\lambda_e S_e}{d_{pe}}\left(T_e^{n+1}\right) + \frac{\lambda_w S_w}{d_{pw}}\left(T_w^{n+1}\right) + + \frac{\rho_P V_p c_p}{\Delta t}\left(T_p^n\right) \tag{35}$$

Now we are done with internal nodes, and so we can move to the **boundary nodes** on top surface of stator.

For **first node**, we have convection on the top side of the wall.

And so:

$$\alpha\left(T_{amb}^{n+1} - T_p^{n+1}\right) = \lambda_s \frac{T_s^{n+1} - T_p^{n+1}}{d_{ps}} \tag{36}$$

In the form of discretization equation:

$$\left[\frac{\lambda_s}{d_{ps}} + h\right]\left(T_p^{n+1}\right) = \frac{\lambda_s}{d_{ps}}\left(T_s^{n+1}\right) + \alpha\left(T_{amb}^{n+1}\right) \tag{37}$$

In the case of the **last node** on the other sides of the mesh we know that the GPM is insulated so:

$$T_p^{n+1} = T_2^{n+1} \tag{38}$$

4.2.3. Equivalent Thermal Conductivity

The electrical insulation in the slot consists of several layers. Each of these layers has different thermal conductivity. An additional thermal contact resistance may exist in the contact surface of these layers. Moreover, in the production, imperfections like air bubbles in the resin, detachment of the resin from the solid surface, etc., can induce additional thermal resistance in the way of heat extraction. To be able to measure the thermal resistance in each layer, the knowledge of temperature in each insulation layer is required, which means a thermocouple should be attached to each layer of insulation. Because of the small thickness of the slot liner and impregnation, the attachment of the thermocouples to them is not feasible. Also, there is no accurate way to predict the effect of manufacturing imperfections. The data that will be obtained from the measurements will be the temperature of the wire and stator surface. With these data in hand, it is possible to calculate the overall thermal resistance of insulation material, i.e. R_{eq}. This equivalent thermal conductivity will include the aggregate effect of all the aforementioned sources. This parameter will be used in the simulations and finally for the comparison of insulation material.

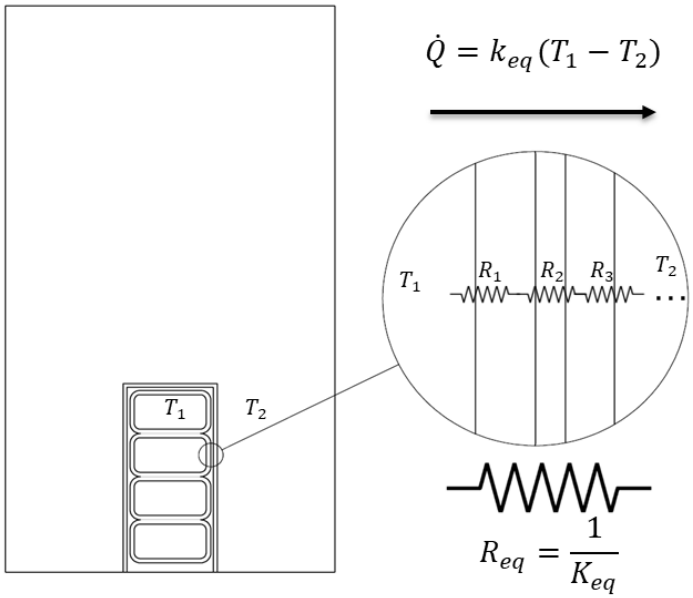

Figure 15. Definition of equivalent thermal resistance for the insulation material

5. Results and Discussion

5.1. Initial Simulation

As explained in chapter 4, for utilizing the experiments to it's fullest, an initial simulation should be performed. The objective of this simulation is to observe the approximate temperature development in the GPM to find out the possible locations for attaching the thermocouples. This model considers all the boundary conditions and heating source to be in their ideal state.

Type of the GPM in this simulation is A-R1. The main parameters in the simulation that are different from the actual experiment and can be major sources of difference are boundary conditions, volumetric heat generation, and equivalent thermal conductivity.

Boundary conditions: In the simulation, all the boundaries of the 2D cross section are thermally insulated other than the top boundary which has natural convection boundary condition. The parameters and conditions in this simulation are presented in Table 4.

Boundary	Boundary condition
Left	Thermal insulation
Right	Thermal insulation
Bottom	Thermal insulation
Top	Natural convection (air)

Table 4. Boundary conditions selected for the model

Volumetric heat generation: Volumetric heat generation is calculated theoretically using Joule effect and is equal to $6.67 \times 10^5 \frac{W}{m^3}$. However, the actual heat generation in the test will be different due to the additional resistance introduced by the electrical connections to the power source. Connection to the power source is through screws. So there will be contact resistance in the connection points.

Thermal conductivity of insulating material: In the simulation, the conductivity of the insulating material is equal to the values extracted from their datasheet. Thermal contact resistance is a major resistance toward heat transfer which has been neglected in this simulation. Moreover, additional imperfections may appear during the production phase that will affect the conduction heat transfer.

Figure 16 demonstrates the temperature contour in the GPM after the steady-state condition has been reached. The temperature within the slot is higher than the temperature in the stator steel. This temperature difference was expected because the copper is the source of heat generation, and the low thermal conductivity of the electrical insulation material in the slot enforces a temperature gradient between wires and the stator steel. To evaluate the overall thermal conductivity of the insulating material, temperature shall be measured in at least two points, one inside the slot and one on the stator.

Considering the accessibility of the locations, the stator top surface and the bottom wire are two feasible spots to attach the thermocouples. Furthermore, temperature contour shows that the temperature is almost identical all over the stator cross section due to the small dimensions of GPM and high thermal conductivity of the electrical steel. Selected spots to attach the thermocouples are shown in Figure 16. It should be noted that the thermocouple on the wire is directly in contact with the copper. Hence, a part of the PEEK layer was removed.

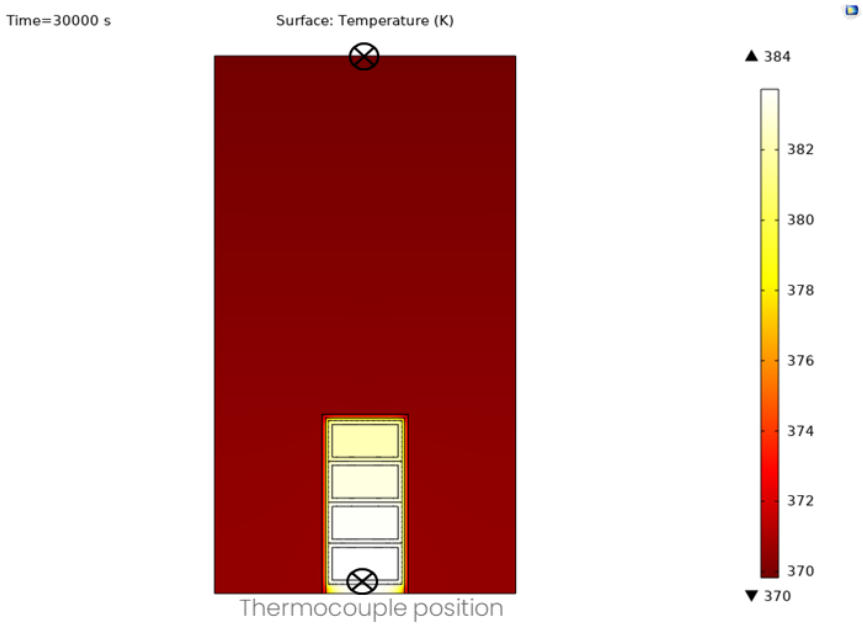

Figure 16. Temperature contour in the steady-state condition - COMSOL

Temperature evolution in the wire and stator is shown in Figure 17. Based on the Figure 17, it can take approximately 8 hours for the GPM to reach stead-state condition.

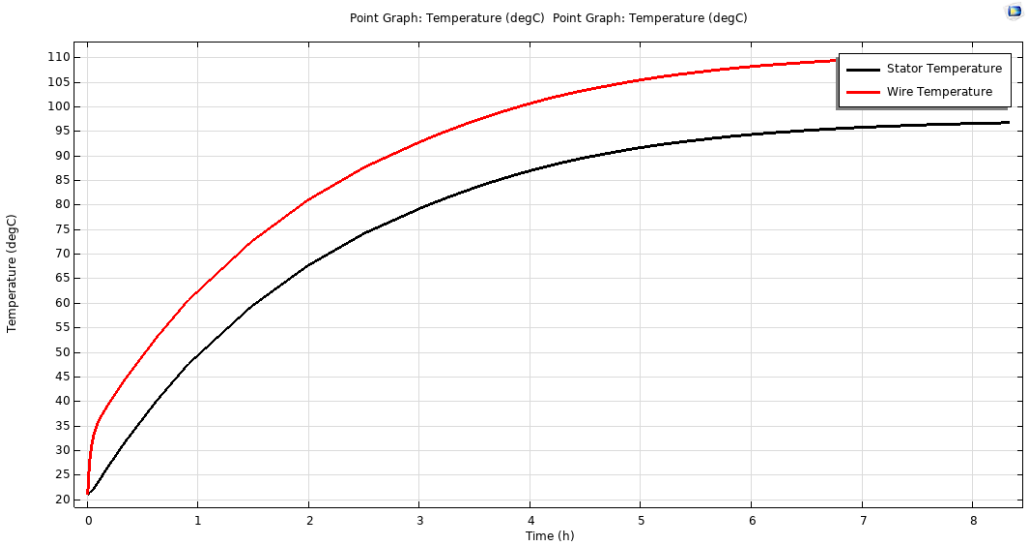

Figure 17. Bottom wire temperature and the stator surface temperature evolution with time

5.2. Test Results

5.2.1. Experiments Before Aging

After thermocouples were attached, thermal measurements of GPMs were started. For the measurement, each pair of GPMs, i.e. GPMs with the same electrical insulating material, were connected in series, and both of them were connected to the power source (Figure 18). It should be noted that in each experiment, the two GPMs are composed of same electrical insulation material but they are not exactly identical. A part of PEEK layer in GPM 1(a) is removed for attaching the thermocouple to the wire which is not the case in GPM 1(b). To reach steady-state, the experiment had to be continued for almost 2 hours, depending on the GPM type. Steady-state condition is very unlikely to happen in an actual electric motor under operation. The main objective of the experiments is to compare different electrical insulating materials' thermal performance in the transient stage. Hence, the thermal measurements for all the GPMs stopped in 1.5 hours. Shortening the experiment time will enable us to increase the number of tests and ensure that the results are repeatable.

Figure 18. Test setup during the experiment

Figure 19 demonstrates temperature measurements in a typical experiment (A-R1). As can be seen from the plot, at the beginning of the test, the temperatures of the GPM start increasing in a fast rate and the increasing rate reduces as the test continues until steady-state has been reached. The increase in the temperature of the wire at the beginning is faster than the stator because of the high thermal resistance of the electrical insulation material. The ambient temperature remains approximately constant during the experiment with a small fluctuation. Hence, the ambient temperature in the simulation is assumed to be constant and equal to the average value of temperature in the experiments. The initial temperature of the GPM is equal to the ambient temperature. Another piece of information that can be extracted from Figure 17 is that the stator temperature in GPM 1(b) is higher than the stator temperature in GPM 1(a).

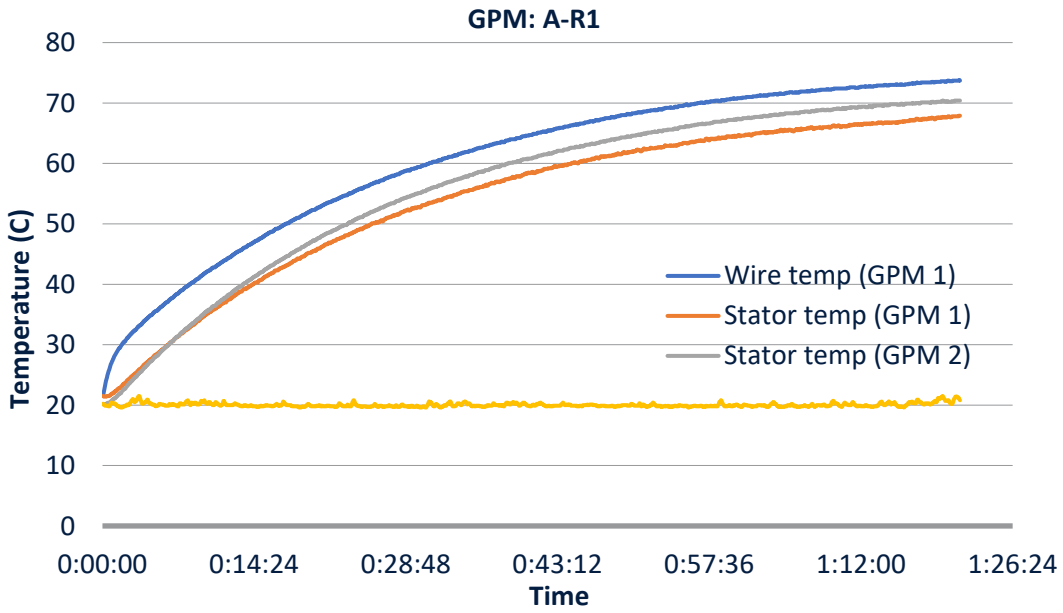

Figure 19. Temperature evolution in the A-R1 type GPM

Figure 20 demonstrates the evolution of temperature in 4 different GPMs. As is depicted in the Figure 20, even though the initial temperature and electrical current passing through the wires is identical in all the cases, the temperature evolution graph is different for each case. It was imagined that the main cause of the difference in temperature profiles is the insulation materials which is different for each GPM. Hence, to ensure the reliability of the results obtained from the experiments, repeatability test was performed. In the repeatability tests, the same pair of GPM went through measurements for several times, while the effort was to maintain identical condition for the experiments. Figure 21 shows the results of three repeated experiment on A-R1 and C-R1. The temperature shown in the plots is wire temperature. It can be seen from the Figure 21 that, even under the identical conditions repeating the measurements for the same set of GPMs will not result in the exact same temperature profile. That means, there are other parameters that are affecting the results and hence, the difference in temperature plots for different GPMs in Figure 20 is not only because of the difference in insulation materials. Therefore, it is necessary to identify these parameters that are affecting the test results and study their effect.

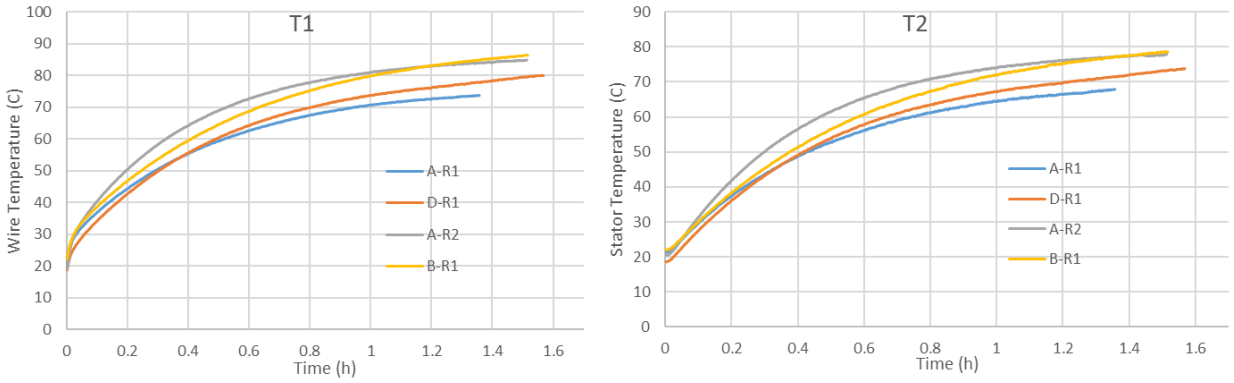

Figure 20. Comparison of wire temperature (left) and stator temperature (right) evolution in 4 different GPMs

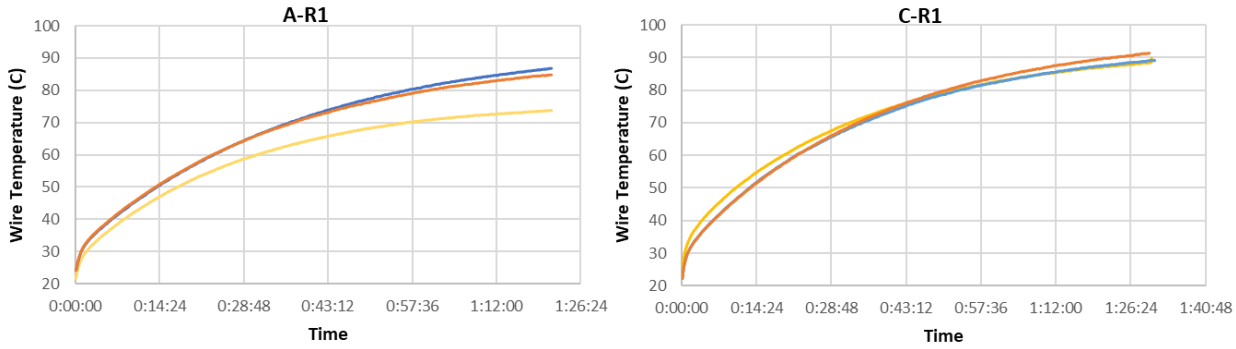

Figure 21. Wire temperature graph for the GPMs, A-R1 and C-R1 after repeating measurement for three times

After performing some tests, it was noticed that the final results are highly dependent on the ambient temperature, quality of connections to the power source, and positioning of the GPM inside insulation box. So, the test was repeated for all the GPMs to ensure that the results were consistent. The duration of each experiment was 1.5 hours. Table 5 summarizes the results of all the experiments that were performed without any problem to the end. In some experiments, the measurements had to be stopped because of the detachment of thermocouples or overheating of the stator. As can be seen from Table 5, repeating the experiments for each GPM will not necessarily result in the same results. After investigating the results, it was noticed that the following parameters are the main source of error in the measurements:

Ambient temperature: It can be seen from Figure 19 that the ambient temperature is constantly oscillating. Fluctuation of temperature is due the reasons such as; opening and closing the laboratory's door, opening an closing the oven's door in the laboratory, and even people passing by the test setup. Moreover, the power source itself generates a significant amount of heat, and this heat is removed by a small fan installed on the power source that turns on and off automatically. The main parameter that is affecting the ambient temperature are two big ovens that are running at high temperature (200 C) and

are used for the thermal aging of electric motors. Moreover, the thermocouple that is measuring ambient temperature is floating in the air and very close to the power source. So, the heat released by the power source periodically is affecting the temperature that thermocouple is sensing.

Insulation box: As explained in section 4.1.3, GPMs are placed inside the insulation box to simulate the boundary conditions in a real segment inside electric motor. However, the insulating box is not a perfect fit for the GPM and there are air layers between the GPM and insulation box's wall. The existing thin air layer between the GPM and box, is producing natural convection effect that is removing the heat. Hence, when placing the GPM inside the box, depending on their position in box, GPMs are experiencing slightly different boundary conditions.

Electrical connections to the power source: To have the electric current in wires inside GPM, two GPMs are connected in series and both are connected to the power source. The connection between GPMs and power source to GPMs is by screw. To have a perfect connections, first, the two connectors should be aligned properly, then screw will ensure that the connectors are properly in contact. Despite the efforts, the connections cannot be identical which means different resistance in GPMs and consequently different heating values in the wires.

GPMs	Average ambient temp (°C)	Wire temp (°C)	Stator Temp (°C) (GPM1)	Stator Temp (°C) (GPM2)
B-R1 - Run1	20.4	85.9	78.2	80.8
B-R1 - Run2	21.2	86.4	78.6	80.5
B-R1 - Run3	22.0	88.4	80.0	86.2
B-R2 - Run1	21.6	83.8	76.5	77.6
B-R2 - Run2	21.6	83.3	75.6	79.3
B-R2 - Run3	22.7	86.6	78.5	85.0
D-R1 - Run1	19.8	95.4	88.7	106.7
D-R1 - Run2	19.5	79.6	73.2	103.3
D-R1 - Run3	20.0	83.8	77.5	80.6
C-R1 - Run1	19.5	89.2	81.5	72.2
C-R1 - Run2	23.6	89.1	82.7	85.2
C-R1 - Run3	23.2	91.4	85.0	85.5
A-R1 - Run1	20.0	73.7	67.9	70.4
A-R1 - Run2	22.6	88.4	82.2	87.7
A-R1 - Run3	22.7	86.1	79.8	84.0
A-R2 - Run1	23.2	84.8	77.8	61.7
A-R2 - Run2	22.6	86.2	77.4	65.2
C-R2 - Run1	19.8	91.5	85.8	77.3
C-R2 - Run2	22.7	90.1	84.8	81.6
D-R2 - Run1	20.0	68.3	63.3	-
D-R2 - Run2	24.2	72.5	68.6	-

Table 5. Average ambient temperature, wire temperature, and stator temperature in GPMs after 1.5 hours of experiment (D-R2 was missing a pair)

The results obtained from the repeated experiments were different. In some cases, the variation was more than in others. Therefore, to be able to compare the GPMs, the average value of the final wire and stator temperature was calculated and presented in Table 6. Figure 22 shows the average value of wire

temperature after repeating the experiments for the different GPMs together with the standard deviation. It can be seen that in some cases, such as B-R1, C-R2, C-R1, and A-R2, the results are very consistent after several measurements. On the other hand, in GPMs like D-R1 and A-R1, the deviation of results from the average value is high. The results show that the D-R2 offers the best cooling performance for the wires.

GPM type	Wire temperature (°C)		Stator temperature (°C)	
	Average	Standard deviation	Average	Standard deviation
B-R1	86.90	1.32	78.93	0.95
B-R2	82.43	4.52	75.23	3.50
D-R1	86.27	8.18	79.80	8.00
D-R2	70.40	2.97	65.95	3.75
C-R1	89.90	1.30	83.07	1.78
C-R2	90.80	0.99	85.30	0.71
A-R1	82.73	7.91	76.63	7.66
A-R2	85.50	0.99	77.60	0.28

Table 6. Average temperatures and standard deviation of results after several experiments for each GPM type

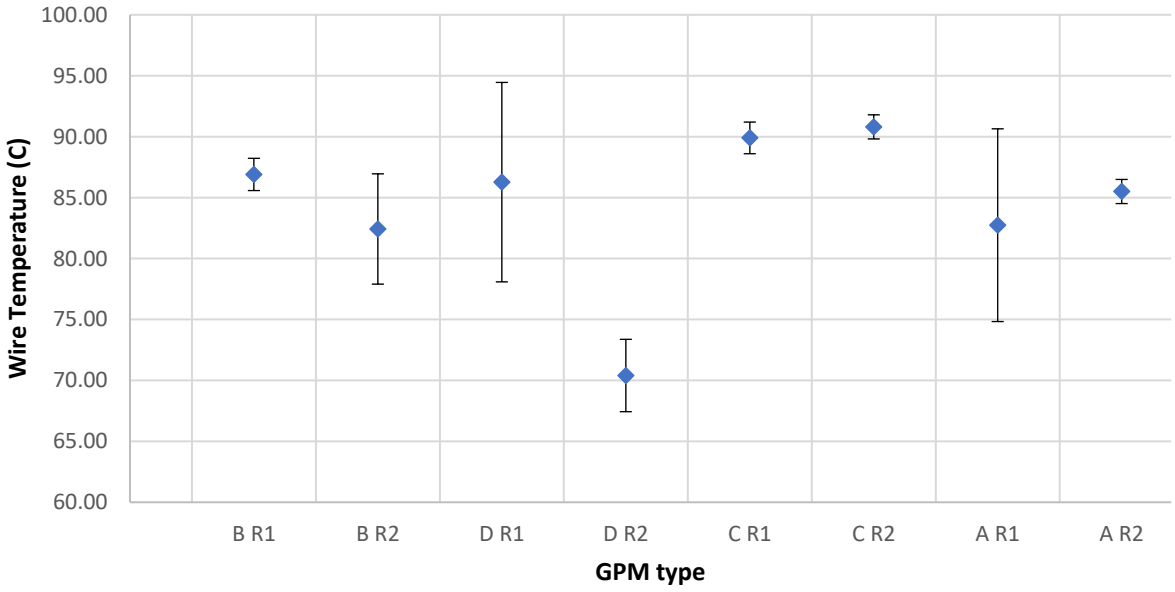

Figure 22. Average wire temperature after several experiments for each GPM type together with standard deviation of results

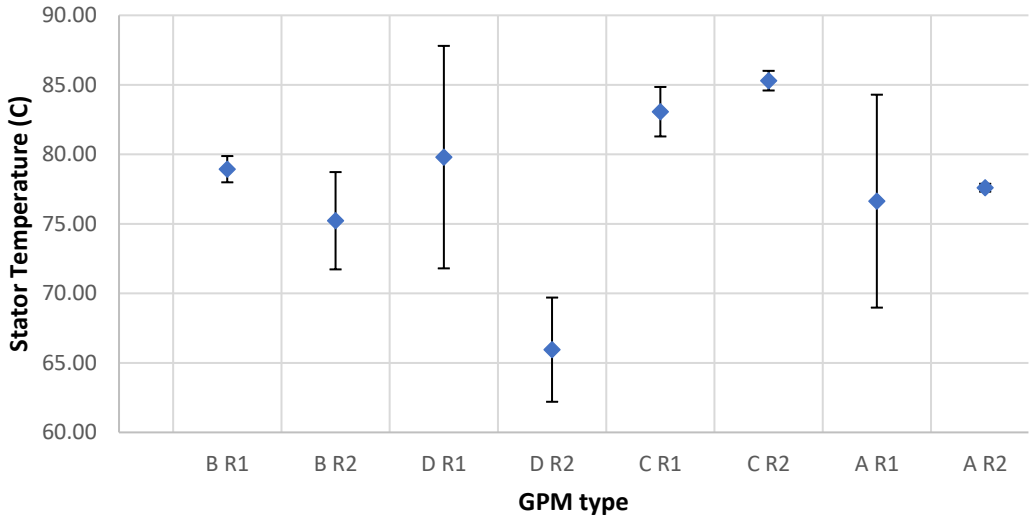

Figure 23. Average stator temperature after several experiments for each GPM type together with standard deviation of results

5.2.2. Wetting and Hydrophilic Surfaces

It was expected that the only parameter that would affect the heat transfer properties inside the slot would be the thermal properties of the insulating material. However, in the production of the GPMs, it was noticed that one important aspect that will determine the effectivity of impregnation in filling up the gaps and avoiding the appearance of air bubbles in the slot is how hydrophilic the liquid impregnation is towards the slot liner's surface. To investigate this phenomenon further, a small droplet of each impregnation was placed on all 4 slot liners, and the picture of the contact area was taken from the side view. The contact angle of impregnation material and the surface of slot liners are demonstrated in Figure 24. In all the cases, the wetting angle is low and the droplet is hydrophilic, with no significant difference between different cases.

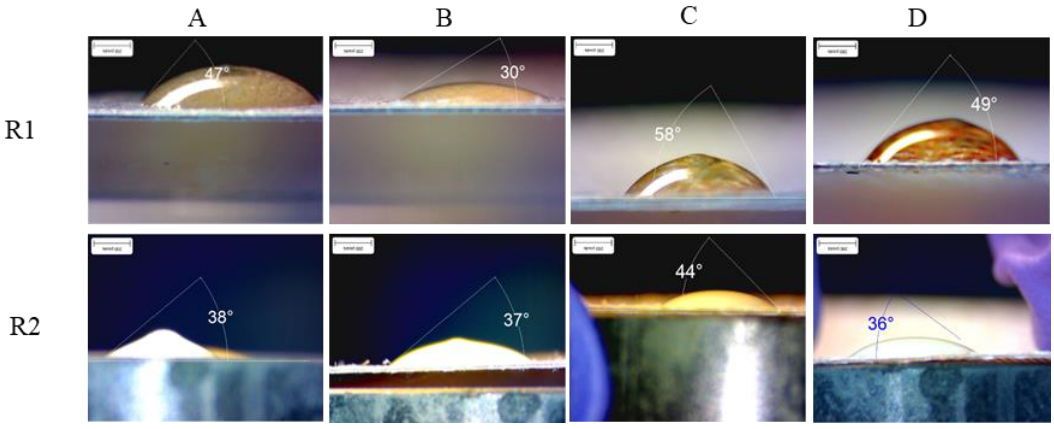

Figure 24. The contact angle of the impregnation materials with the slot liner's surface

After this experiment, it was noticed that another aspect of the interaction between impregnation and the slot liner could be the absorptivity of the slot liners in contact with impregnation. In this case, when the slot liner is in contact with impregnation in its liquid phase, before curing temperature, impregnation will penetrate and fill some of the gaps inside the slot liner. Since these gaps are initially filled with air, absorption of the impregnation will improve the thermal conductivity in the slot liner. Figure 25 shows the absorptivity of slot liners in contact with impregnation material. It is evident that the D and C have a better absorptivity compared to A and B. In the case of impregnations, the R2 (white droplet) is absorbed better for the same slot liner.

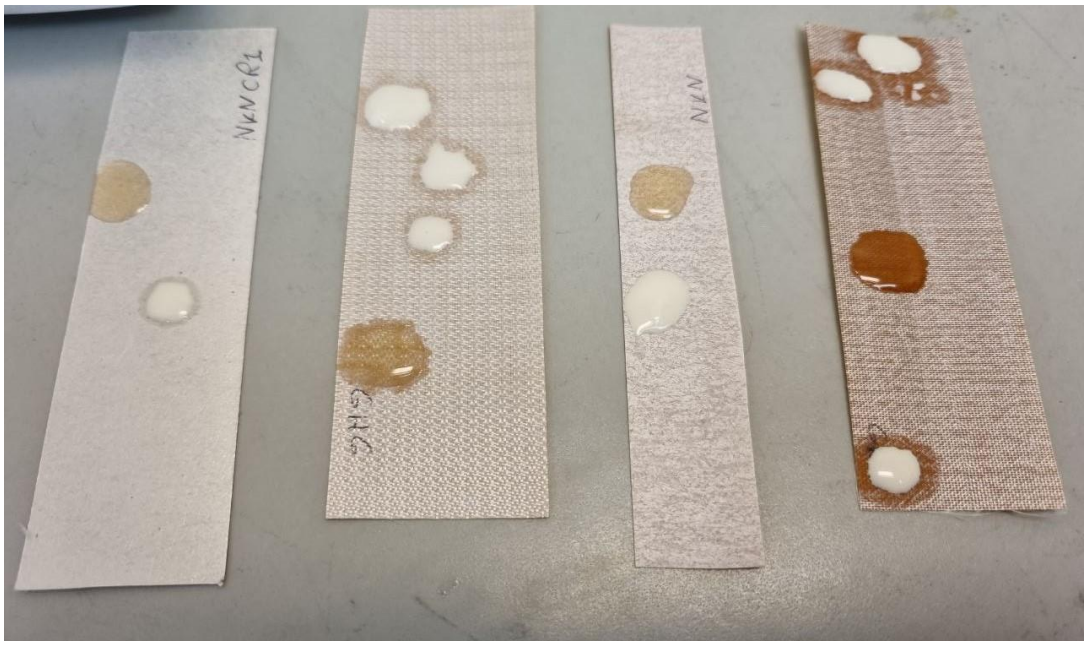

Figure 25. Comparison of absorptivity of slot liners in contact with liquid impregnation. Slot liners in the picture from left to right are B, D, A, C. Impregnation with the white appearance is R2

5.2.3. Thermal Aging

After finishing the initial thermal tests on the GPMs, GPMs were placed inside the oven to go through the thermal aging process. The objective of the thermal aging was to observe if there will be any significant change in the thermal and electrical performance of insulating materials after they have gone through thermal stress for a long time. Therefore, GPMs were placed inside the oven for 500 hours and at 200 C, which is a standard thermal aging procedure for electric motors. According to a rule of thumb each 10 C of increase in temperature compared to the normal operating temperature halves the life expectancy of the electric motor [16]. The operating temperature in electric motors under extreme conditions can increase up to 120 C [17]. Hence, using the rule of thumb, the thermal aging at 200 C for 500 hours is approximately equivalent to 50000 hours of operation of the electric motor in 133.5 °C.

5.2.4. Experiments After Aging

GPMs have gone through thermal aging after being in the oven for approximately three weeks. Because of the high temperature, thermocouples attached to the stator's surface came off. So, all the thermocouples needed to be attached before starting the experiments. The experiment setup is exactly how it was for the thermal measurements before aging. The effort was to keep the changes in the test setup to a minimum so the changes in the temperatures would be only due to the thermal aging of the insulation layer. Again, to ensure the reliability of the results, the experiments was repeated 3 times for each pair of GPMs. The average ambient temperature, and the final temperature of the wire, stator (GPM1), and stator (GPM2) at the end of 1.5 hours of experiment is presented in Table 7.

GPMs	Average ambient temp (°C)	Wire temp (°C)	Stator Temp (°C) (GPM1)	Stator Temp (°C) (GPM2)
B-R1 - Run1	24.0	85.0	77.5	82.7
B-R1 - Run2	25.3	89.3	81.9	84.1
B-R1 - Run3	26.2	88.0	80.9	82.9
B-R2 - Run1	25.3	90.6	81.5	92.7
B-R2 - Run2	25.1	95.5	87.4	88.4
B-R2 - Run3	25.0	90.2	81.3	94.3
D-R1 - Run1	25.9	86.4	80.1	79.9
D-R1 - Run2	26.2	99.8	92.6	87.5
D-R1 - Run3	24.8	86.8	80.5	79.5
D-R2 - Run1	25.6	73.8	69.9	-
D-R2 - Run2	28.0	72.2	68.3	-
D-R2 - Run3	24.0	69.8	65.8	-
A-R1 - Run1	26.3	85.5	77.2	81.3
A-R1 - Run2	25.6	87.1	78.4	82.3
A-R1 - Run3	23.7	84.0	76.0	80.8
A-R2 - Run1	26.2	91.5	79.6	84.0
A-R2 - Run2	25.4	89.2	77.0	81.9
A-R2 - Run3	25.8	89.9	77.8	83.1
C-R2 - Run1	25.3	98.2	89.1	102.1
C-R2 - Run2	25.5	89.1	81.9	97.1
C-R2 - Run3	23.9	87.7	80.4	93.1
C-R1 - Run1	24.67	85.3	78.5	85.8
C-R1 - Run2	25.57	86.5	79.7	83.9
C-R1 - Run3	24.96	83.7	76.7	81.5

Table 7. Average ambient temperature, wire temperature, and stator temperature in aged GPMs after 1.5 hours of experiment

Due to the parameters mentioned in section 5.2.1, which were causing inconsistency in the results, all the experiments for each pair of GPM were repeated three times. To reduce the large amount of data, Table 8 summarizes the average values obtained for each GPM and the standard deviation in the results.

These average temperature values are visualized in Figure 26 and Figure 27 for wire temperature and stator temperature respectively.

GPM type	Wire temperature (°C)		Stator temperature (°C)	
	Average	Standard deviation	Average	Standard deviation
B-R1	87.43	2.21	80.10	2.31
B-R2	92.10	2.95	83.40	3.47
D-R1	91.00	7.62	84.40	7.10
D-R2	71.93	2.01	68.00	2.07
C-R1	85.17	1.40	78.30	1.51
C-R2	91.67	5.70	83.80	4.65
A-R1	85.53	1.55	77.20	1.20
A-R2	90.20	1.18	78.13	1.33

Table 8. Average temperatures and standard deviation of results after several experiments for aged GPMs

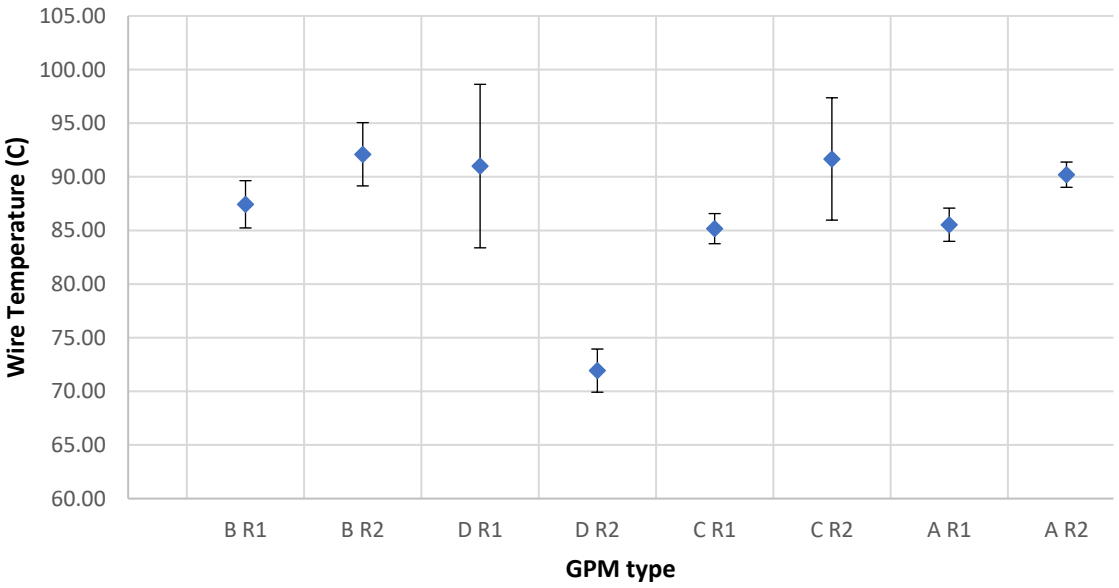

Figure 26. Average wire temperature after several experiments for each GPM type together with standard deviation of results after aging

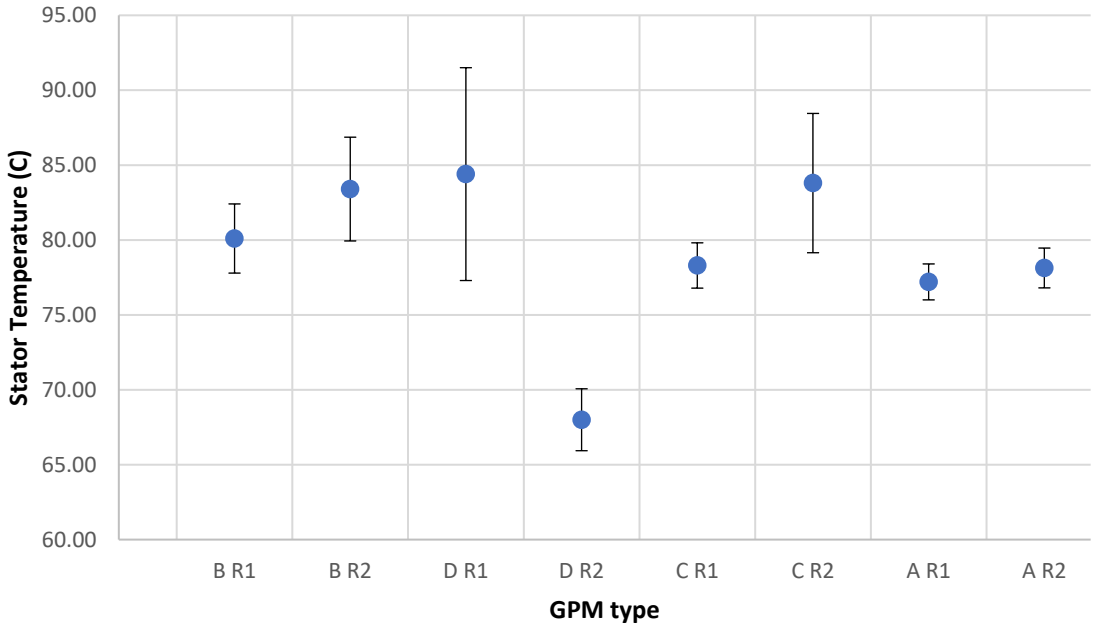

Figure 27. Average stator temperature after several experiments for each GPM type together with standard deviation of results after aging

One may think that the average temperature of the wire at the end of the experiment can be a good indicator for the comparison of the conductive cooling performance of the insulating material. Average wire temperature, indeed, can be a good indicator if the other parameters that are affecting the results have been kept identical, i.e. heating and convection coefficient. Some of these parameters, such as electrical connections and positioning the GPM inside the insulation box, are extremely hard to control. Even if these parameters are kept identical, ambient temperature is clearly different in experiments before and after aging (Figure 28). Due to the lack of compatible air conditioning and operation of ovens in the room, the room temperature after aging is significantly higher than the room temperature before aging. The ambient temperature significantly affects the final temperatures reached in GPMs at the end of the experiment. Hence, wire temperature alone cannot be an accurate indicator for comparing the GPMs with each other and GPMs before and after aging.

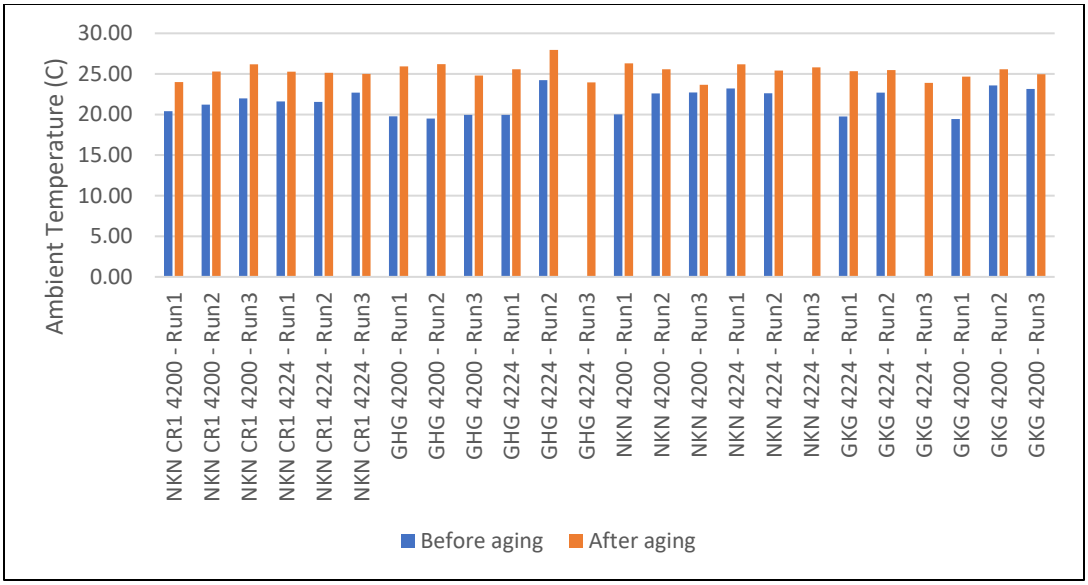

Figure 28. Average ambient temperature during the each experiment, before and after aging

5.3. Simulations

5.3.1. Verification of the Models

Looking at the results obtained from the experiments, it is evident that there is a huge difference between the simulation and the experiments. After investigation of the results and performing sensitivity analysis in the simulations, it was observed that the main reasons that caused the difference between the simulations, which were done in an ideal environment, and actual experiments were mainly due to the three parameters:

Natural convection heat transfer coefficient: It was explained in the previous sections that in order to simulate the thermal insulation boundary condition, the GPMs are embedded inside an insulation box which is 3D printed. In the initial simulation, the boundary condition of the side walls was thermal insulation (Figure 12). However, in the actual situation, when the GPM is placed inside the insulation box, there is a small layer of air which is filling up the gap between the GPM and the insulation box. This small layer is enough to have a natural convection effect on both sides of the GPM. In the initial model, the time needed to reach steady-state condition was almost 8 hours. But, in the experiments, it was observed that the temperature in GPMs will stabilize after approximately 2 hours. A sensitivity analysis was performed to find out the origin of this difference. It was noticed that steady-state time is related to the physics of the problem, i.e. boundary conditions. By increasing the natural convection coefficient, the GPM's interaction with the ambient will increase and consequently, the steady-state condition will arrive faster (Figure 29). Therefore, the steady-state time in the actual experiment is shorter than in the simulation

because of the additional convection heat transfer inside the insulation box that wasn't taken into consideration in the simulation. To take into account this difference, in the simulation, the side walls boundary condition that was initially thermal insulation was replaced by natural convection. The values of the HTC is adjusted until the simulation model reaches the steady-state at the same time as the tests.

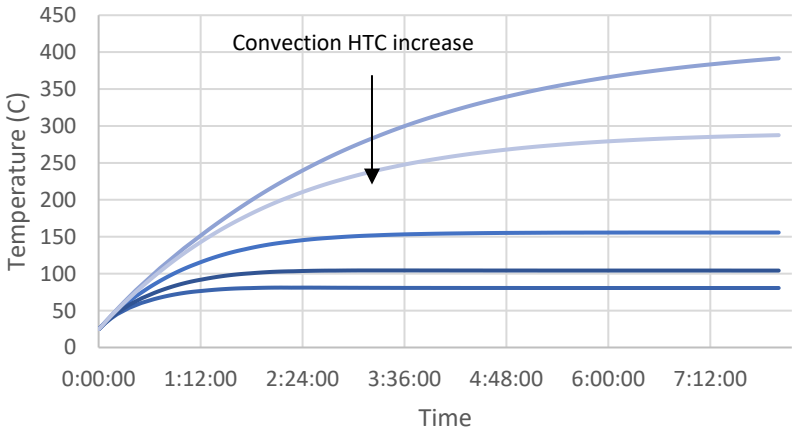

Figure 29. Effect of natural convection coefficient variation on steady-state condition time (stator temperature)

Joule heating value: The value of natural convection HTC was determined using the time that it takes to stabilize the temperature. Next step is to determine the accurate value of Joule heat generation in the wires. The heat generation value depends on the current and the resistance of the wire. The value of current was adjusted to be 60A for all the measurements using power source. However, depending on the length of wire, effectivity of soldering, and the screw connections to the power source, each GPM had a different resistance and consequently a different heat generation value. Performing sensitivity analysis showed that the stator temperature value is mainly a function of volumetric heat generation and the equivalent thermal resistance of insulation material has a negligible effect on it (Figure 30). Hence, the stator temperature can be used to set the value of volumetric heat generation in the simulation.

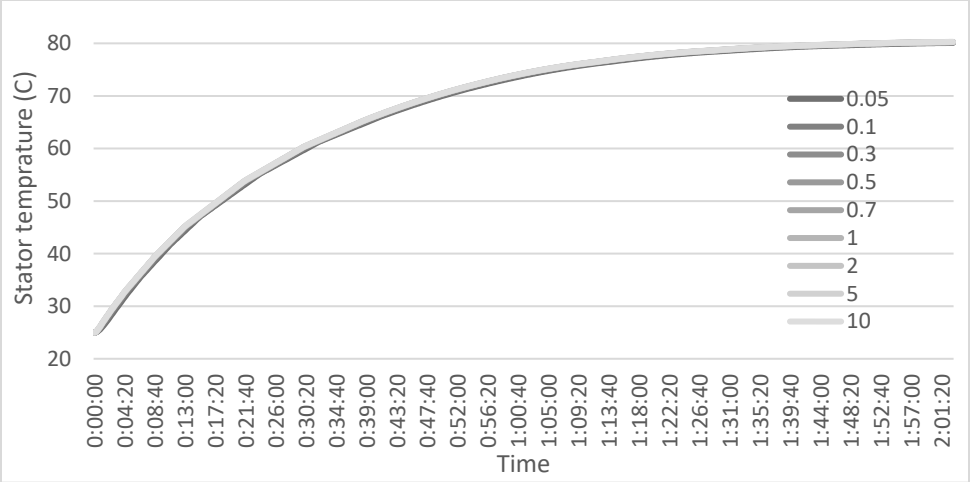

Figure 30. Effect of k_{eq} of insulation material on the evolution of stator temperature for a constant heating

Equivalent thermal conductivity: The third step in finalizing the simulation is to utilize the wire temperature obtained from the measurements to evaluate K_{eq}. By increasing K_{eq} wire temperature will decrease because generated heat is removed more effectively from the slot. Figure 31 shows the effect of K_{eq} on the evolution of wire temperature.

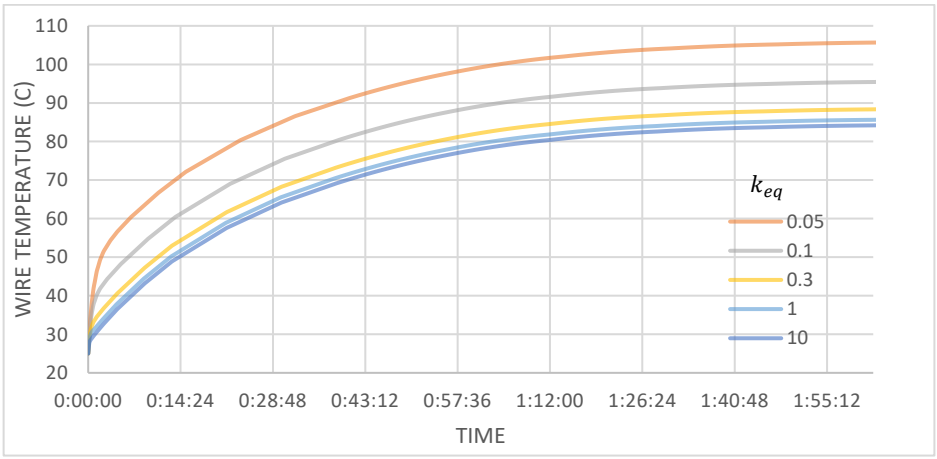

Figure 31. Effect of K_{eq} on the evolution of wire temperature for a constant heating value

In summary, with three steps, simulations can be fitted to the specific GPM in experiment. These three steps are:

- Finding the right value for the natural convection coefficient using the steady-state time
- Finding the heat generation using stator temperature
- Evaluating K_{eq} using wire temperature

Figure 32 shows the temperature contour in the cross section of the GPM (A-R1). Other than changes in volumetric heat generation and thermal conductivity, more geometrical details has been added to the model. From the contour it appears that the highest temperature in the cross section is achieved in the third wire (from top). The temperature is almost uniform in the stator.

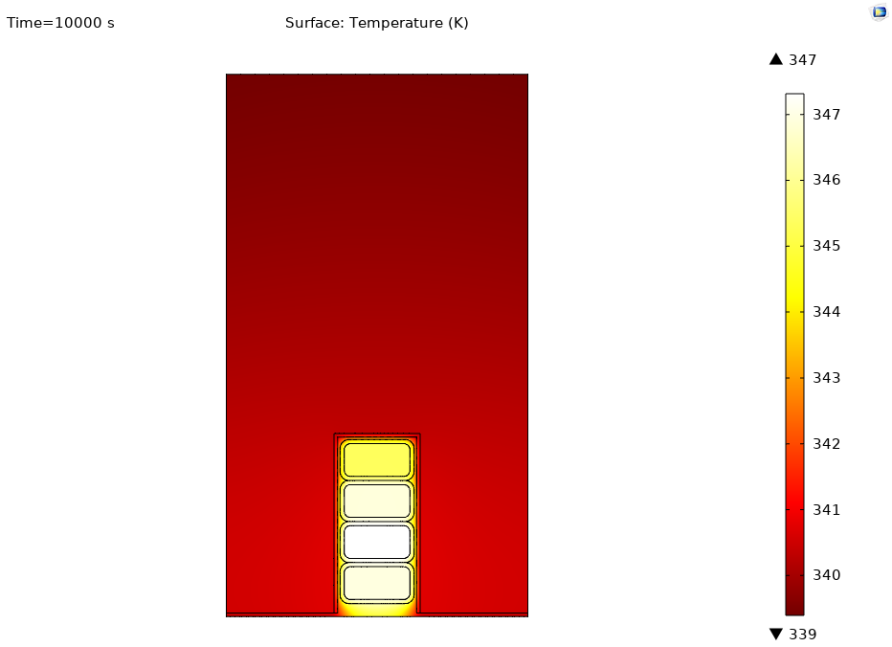

Figure 32. Temperature contour of the A-R1 in the steady-state condition – COMSOL

The temperature contour, obtained from the MATLAB simulation is shown in Figure 33. The number nodes used for this simulation is 31×31. Gauss-Seidel convergence criteria is $1e-5$.

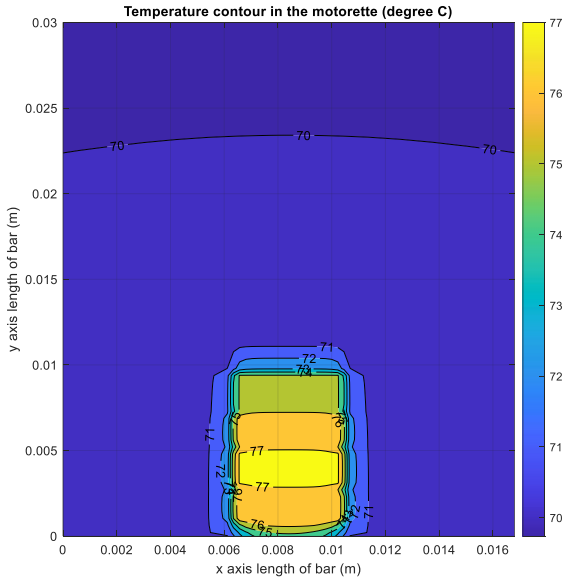

Figure 33. Temperature contour of the A-R1 in the steady-state condition – MATLAB model

5.3.2. Utilizing Models

By following the steps that were explained previously, COMSOL and MATLAB models can be adjusted for each experiment to give the same results (Figure 34). Validated simulations can predict the steady-state temperature with being have to continue the experiment. The beginning of the experimental plot will be enough to adjust the model for that specific measurement. Moreover, since simulations can be adjusted specifically to each measurement, it is possible to evaluate the accurate value of k_{eq} for each GPM.

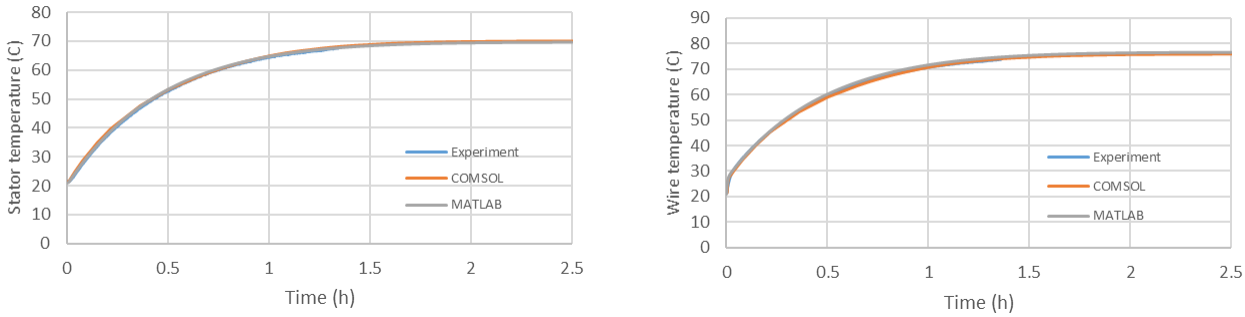

Figure 34. Comparison of temperature evolution in experiment, COMSOL, MATLAB

The equivalent thermal conductivity of each GPM, before and after aging is shown in Table 9. It can be observed that, D and C slot liners have a better thermal conductivity. D-R2 in particular has the highest value of thermal conductivity.

GPM	Thermal conductivity	
	Before aging	After aging
B-R1	0.35	0.45
B-R2	0.3	0.27
D-R1	0.5	0.72
D-R2	0.87	0.64
C-R1	0.53	0.55
C-R2	0.57	0.42
A-R1	0.59	0.29
A-R2	0.42	0.145

Table 9. Thermal conductivity of each GPM. Before and after aging

5.4. SEM/EDS Analysis

It was observed in Table 9 that D-R2 has the highest thermal conductivity. The improvement in thermal conductivity of R2 resin compared to R1 is mainly due to the thermal fillers (Aluminum oxide particles) inside the R2 resin. When resin R2 is in the liquid state, these particles will accumulate in the pot's bottom. Hence, before using the R2, it should be ensured that these particles are evenly distributed in the resin by stirring the resin. To ensure that the aluminum oxide particles had reached to all the spots inside the slot, we decided to cut one of the GPMs, which was made of R2 resin and started to investigate the cross-section using a Scanning Electron Microscope (SEM) (model: Zeiss Sigma VP). Figure 35 shows the magnified pictures of the electrical insulation layer in two different locations. These pictures are taken from C-R2 cross-section with SEM. In these pictures, some examples of manufacturing defects such as air bubbles and resin separation from the stator surface can also be seen. Energy-dispersive X-ray Spectroscopy (EDS) (model: Aztec, Oxford Instruments) analysis was also performed to find out the elements in the slot. Based on the results, the main elements in the slot are Fe, Cu, Si, C, Al, and Ca. The element that is interesting for us in this analogy is Al. Aluminum in the slot is coming from the Aluminum oxide particles in the R2 impregnations. Figure 35 shows that Aluminum oxide particles are perfectly distributed throughout the slot, in all the places that resin exists. It should be noticed that these pictures are from the end of the slot, which is the location that Aluminum oxide particles are less likely to reach.

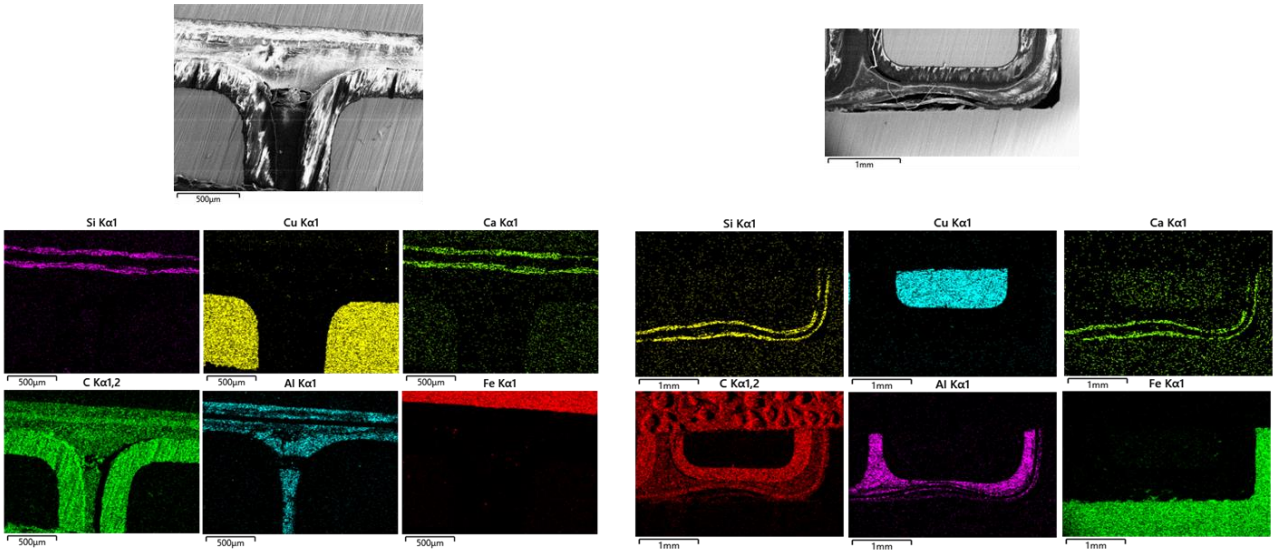

Figure 35. SEM analysis pictures on top together with EDS maps showing distribution of elements

6. Conclusion

Performing the thermal measurement in the laboratory proved to be more challenging than what initially thought. It was difficult to provide identical conditions for all the experiments due to the external parameters that were not controllable. Ambient temperature, insulation box, and electrical connections were the three main affecting parameters in the measurement. Due to the operation of ovens that are used for thermal aging and the lack of proper air condition in the laboratory, the room temperature was different in each experiment. Natural convection heat transfer is proportional to the temperature difference between the stator and the ambient. Hence, different room temperatures resulted in different values of heat transfer to the ambient, which directly affected the final temperature values in the GPM. The physics of the problem, or more specifically, geometry and the boundary condition, will define the form of temperature evolution with time. All the GPMs were similar in their geometries. However, they were experiencing different boundary conditions due to the insulation box. When placed inside the insulation box, GPM, is experiencing different boundary conditions for the side walls. It's neither perfect insulation nor natural convection but something in between which is impossible to repeat that condition exactly. Electrical connections are the last source of inconsistencies. Electrical connections refer to both the solder between wires and screws. These electrical connections were different for each GPM, which can cause different heat generation values in the GPMs. All the errors induced by these parameters made it almost impossible to compare the cooling performance of the GPMs solely by looking at the final temperatures at the end of the experiment.

The initial simulation results obtained from the models were very different from what we observed in the experiments. The unknown parameters that needed to be revaluated in our models based on the results obtained from experiments were natural convection HTC of the side walls, volumetric heat generation, and k_{eq}. Natural convection HTC was estimated using the time that GPM becomes steady-state in the experiments. By increasing the convection coefficient, the time that GPM reaches steady-states decreases. It was also observed that the stator temperature only depends on volumetric heat generation and is not affected by the thermal conductivity of insulation material. Hence, stator temperature was used to estimate the actual value of heat generation. Finally, the value of k_{eq} was evaluated using the temperature difference between the wire and the stator. Therefore, in three steps, simulation models were validated and perfectly simulated the temperature evolution in the actual experiment condition.

Validated models proved to be valuable tools during this project. After the model is validated, it can be used to extrapolate the temperature evolution plot by extending the simulation time to observe the steady-state temperatures. This further helped us to shorten the experiment's time which normally can go up to 2~3 hours, just enough to validate our model. The second advantage that models were offering was the evaluation of k_{eq} for each GPM in the specific test condition for that GPM. Figure 36 shows the equivalent thermal conductivity of each GPM before and after aging. It appears that four GPMs of D-R1, D-R2, C-R1, and C-R2 have the best thermal conductivity and, hence, best cooling performance. A-R1 has a considerable drop in conductivity after aging. The highest overall thermal conductivity belongs to D-R2.

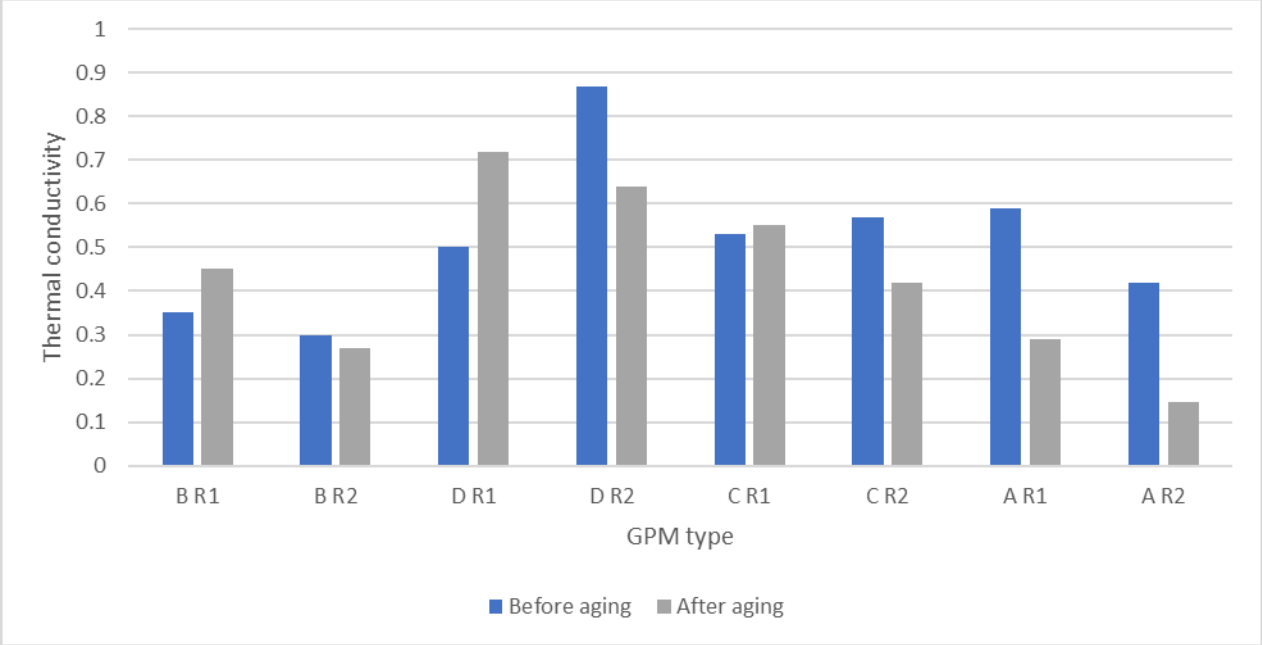

Figure 36. Values of k_{eq} for each GPM type, before and after aging

In the production of GPMs, it was noticed that C has pre-bending problems, making the manufacturing of stators with this slot liner harder than usual. The distribution of thermal fillers inside the R2 impregnation was also investigated during the thesis. It was confirmed that Aluminum oxide particles are well distributed inside the slide. Hence, D-R2 combination is a reliable choice for the insulation material.

Another conclusion that can be drawn from Figure 36 is that thermal aging in general increases the thermal conductivity of the GPMs that are made with R1 impregnation, and it has the opposite effect on the thermal conductivity of the GPMs made with R2 impregnation. This matter requires further investigation. However, an initial guess is that in the case of R1, the resin is expanding due to the aging and is filling up the air gaps inside the slot. For the R2 impregnation, since the Aluminum oxide particles have a different thermal expansion coefficient than the resin, small cracks may appear inside the impregnation after expansion.

Thermal conductivity of electrical insulation materials, separately, cannot specify the heat transfer performance of the combined electrical insulation layer after production. We observed that parameters such as surface tension and viscosity of impregnation, the interaction of impregnation and slot liner in the proximity of each other and all the difficulties experienced in the production phase would affect the overall heat transfer performance of each combination.

7. Future Work

Improving the test results

During the thermal measurements, several sources of error in our measurement was discovered. In general there are three suggestions to improve the experiments:

- **Better control of room temperature**: Installation of adequate air conditioning or performing the experiments in an environment with a controlled temperature can greatly improve the results.
- **Removing the insulation box**: Insulation box is providing inconsistent boundary condition in each experiment. As long as the objective is comparison of insulation material, removing insulation box should not be a problem.
- **Better electrical connections**: Improved electrical connections can avoid external and unpredicted heat generation in the GPM.

Comparing the thermal conductivity with slope

Another approach for comparing the thermal conductivity of insulation material, is to use the slope of the wire temperature evolution graph with time. The higher the slope of the graph the higher the thermal resistance will be. Figure 37 demonstrates fitting of a 4th order polynomial plot to the experimental data. However to be able to use this approach, three conditions should be satisfied in the test environment.

- All the experiments should have exactly the same boundary condition and geometry.
- Ambient temperature should be the same for all the experiments
- And the value of Joule heat generation should be equal for all of the GPMs in experiment

If any of this conditions is not satisfied during the experiments, comparison of the temperature plot slope will be pointless.

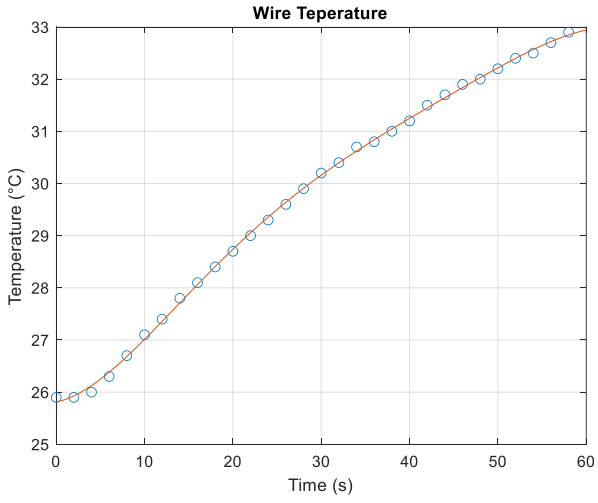

Figure 37. Wire temperature evolution data with the fitted polynomial plot

8. Acknowledgement

First and foremost, I would like to show my gratitude to my supervisor, Anders Thibblin, for giving me the opportunity to perform my master thesis in Scania. The project has for sure increased my knowledge of both theoretical and practical work. I appreciate all the help and support that I have received from him.

Also, I want to thank Tiva Sharifi, which was co-supervising my Master's thesis here. I appreciate all the continuous help and support that I received from her during this Master's thesis.

Moreover, I want to thank my academic supervisor Eugenio Schillaci for the constructive feedbacks that he provided during this time.

I am grateful for all the help I received from Christina Kyrizaki and Felix Pogats, two other Master's students working closely with me in the lab.

I want to thank Heathcliff Demaie and LEMTA - Université de Lorraine for providing the COMSOL license for this work.

And finally, I want to show my deepest gratitude to Fabrice Lemoine, head of the DENSYS program, for giving me the opportunity of being in this wonderful Master's program in the first place, and for his amazing performance and support in this 2 years.

9. Bibliography

[1] "Our electrification roadmap," [Online]. Available: https://www.scania.com/group/en/home/sustainability/sustainable-transport/electrified-solutions/our-electrification-roadmap.html.

[2] "Scania's electrification roadmap," [Online]. Available: https://www.scania.com/group/en/home/newsroom/news/2021/Scanias-electrification-roadmap.html.

[3] *Williamson, S. J., Wrobel, R., Booker, J. D., Yon, J., & Mellor, P. H. (2016). Effects of insulation ageing on the conductive heat transfer from the winding body into machine periphery/stator core pack..*

[4] *Liu, M., Li, Y., Ding, H., & Sarlioglu, B. (2017, June). Thermal management and cooling of windings in electrical machines for electric vehicle and traction application. In 2017 IEEE Transportation Electrification Conference and Expo (ITEC) (pp. 668-673)..*

[5] "Tüysüz, Arda, et al. "Advanced cooling methods for high-speed electrical machines." IEEE transactions on industry applications 53.3 (2017): 2077-2087.".

[6] "Popescu, M., Staton, D., Boglietti, A., Cavagnino, A., Hawkins, D., & Goss, J. (2015, March). Modern heat extraction systems for electrical machines-A review. In 2015 ieee workshop on electrical machines design, control and diagnosis (wemdcd) (pp. 289-296".

[7] "Kulan, M. C., Şahin, S., & Baker, N. J. (2020). An overview of modern thermo-conductive materials for heat extraction in electrical machines. IEEE Access, 8, 212114-212129.".

[8] *Seilmayer, M., & Katepally, V. K. (2018). Thermal conductivity survey of different manufactured insulation systems of rectangular copper wires. AIMS Electronics and Electrical Engineering, 2(1), 27-36..*

[9] "Researchgate," [Online]. Available: https://www.researchgate.net/publication/336846748_Digital_proportional_amplifier_of_linear_DC_electromagnet.

[10] *Rönnberg, K. (2020). Heat-transfer simulations applied to electrical machines (Doctoral dissertation, KTH Royal Institute of Technology)..*

[11] C. V. Salimath, "Thermal Testng and Thermal Modeling of Electrical Insulation System in Electric Machines," 2021.

[12] S. M. I. X. Z. Y. C. X. H. M. I. Qinfen Lu, "Modeling and Investigation of Thermal Characteristics of a Water-Cooled Permanent-Magnet Linear Motor," [Online].

[13] *Dakin, T.W. (1948). Electrical Insulation Deterioration Treated as a Chemical Rate Phenomenon. Transactions of the American Institute of Electrical Engineers, 67, 113-122..*

[14] [Online]. Available: https://www.sciencedirect.com/topics/engineering/radiation-heat-transfer.

[15] T. L. B. F. P. I. D. P. D. A. S. L. T. L Bergman, Fundamentals of Heat and Mass Transfer, John Wiley & Sons, 2011.

[16] "Yang, Yinye, et al. "Thermal management of electric machines." IET Electrical Systems in Transportation 7.2 (2017): 104-116.".

[17] [Online]. Available: https://www.orientalmotor.com/ac-motors-gear-motors/technology/temperature-rise-and-life-of-an-ac-motor.html.

10. Appendix

10.1. MATLAB Code

```
%% Dimensions are removed from the code for confidentiality reasons
%% Clearing data
clear
clc

%% Thermophysical Data Input
% geometry
L ; % length in x direction
H ; % hight in y direction
W ; % 2D

% constant material propertie
% stator
rho_s = 7730; % Kg/m^3
k_s = 40; % W/m/K
cp_s = 465; % J/Kg/K

% wire
rho_w = 8960; % Kg/m^3
k_w = 400; % W/m/K
cp_w = 385; % J/Kg/K
% qv_w = 3e6; % volumetric heat generation by joule effect (W/m^3)
qv_w = 26.5e5;
%Peek / impregnation / slot liner
rho_p = 1300; % Kg/m^3
k_p = 0.23; % W/m/K
cp_p =300 ; % J/Kg/K

% %slot liner
% rho_l = 100; % Kg/m^3
% k_l = 1; % W/m/K
% cp_l =1 ; % J/Kg/K
%
% %impregnation
% rho_i = 100; % Kg/m^3
% k_i = 1; % W/m/K
% cp_i =1 ; % J/Kg/K

T_initial = 21; % intial temperature
T_amb = 21; % ambient temperature
alpha = 25; % heat convection
alpha_s = 8;
%% Numerical data
delta = 4e-5; % convergence criteria
N = 31;
```

```
M = 31;
fr = 1; % Relaxation factor
dt = 10; % time step (s)
final_time = 1.5*3600; % simulation time (s)

%% Mesh generation

x_p = zeros(1,N+2);
y_p = zeros(1,M+2);
V = zeros(N+1,M+1);
T = ones(N+2,M+2)*T_initial;
T_prev = T;

% mesh distribution on x axis
x1 = linspace(0,6e-3,N/6+1);
x2 = linspace((6+*6/4/N)*1e-3,e-3,4*N/6+1);
x3 = linspace((6*6/N)*1e-3,e-3,N/6);
x_cv = cat(2,x1,x2,x3);

% mesh distribution on y axis
y1 = linspace(0,10e-3,5*M/6);
y2 = linspace((10+20*(1/(M/6+2)))*1e-3,30e-3,M/6+2);
y_cv = cat(2,y1,y2);

[X,Y]=meshgrid(x_cv,y_cv);
hold on;
plot(X,Y,'k');
plot(X.',Y.','k');


for i = 2:N+1
    x_p(i) = (x_cv(i) + x_cv(i-1))*0.5;
end
for i = 2:M+1
    y_p(i) = (y_cv(i) + y_cv(i-1))*0.5;
end

for i = 2:N+1
    for j = 2:M+1
        V(i,j) = (x_cv(i) - x_cv(i-1)) * (y_cv(j) - y_cv(j-1)) *1 ;
    end
end

x_p(1) = 0;
y_p(1) = 0;
x_p(N+2) = L;
y_p(M+2) = H;
[X,Y] = meshgrid(x_p,y_p);
%% Material properties assignment
rho = ones (N+2,M+2)*rho_p;
k = ones (N+2,M+2)*k_p;
cp = ones (N+2,M+2)*cp_p;
qv = zeros (N+2,M+2);
for i = 1:N+2
```

```
    for j = 1:M+2

        % steel
        if x_p(i)<6e-3 || x_p(i)>10.8e-3 || y_p(j)>10e-3
            rho(i,j) = rho_s; % density
            k(i,j) = k_s; % thermal conductivity
            cp(i,j) = cp_s; % heat capacity
        end

        % wire

        if (6.5675e-3 < x_p(i)) && ( x_p(i)< 10.2325e-3) && (((0.7525e-3 < y_p(j)) &&
( y_p(j)< 2.5775e-3)) || ((3.0375e-3 < y_p(j)) && ( y_p(j)< 4.8625e-3)) || ((5.3225e-
3 < y_p(j)) && ( y_p(j)< 7.1475e-3)) || ((7.6075e-3 < y_p(j)) && ( y_p(j)< 9.4325e-
3)))
            rho(i,j) = rho_w; % density
            k(i,j) = k_w; % thermal conductivity
            cp(i,j) = cp_w; % heat capacity
            qv(i,j) = qv_w; % volumetric heat generation by joule effect
        end


    end
end

%% Discretization coefficient

a_E = zeros(N+2,M+2);
a_W = zeros(N+2,M+2);
a_N = zeros(N+2,M+2);
a_S = zeros(N+2,M+2);
a_P = zeros(N+2,M+2);
b_P = zeros(N+2,M+2);

k_e = zeros(N+2,M+2);
k_n = zeros(N+2,M+2);
k_s = zeros(N+2,M+2);
k_w = zeros(N+2,M+2);
% middle nodes
for i=1:N+2
    for j=1:M+2

        if j == M+2
            %           d_PE = x_p(i+1) - x_p(i);
            %           d_PW = x_p(i) - x_p(i-1);
            d_PS = y_p(j) - y_p(j-1);

            %           s_e = y_cv(j) - y_cv(j-1);
            %           s_w = y_cv(j) - y_cv(j-1);
            %           s_n = x_cv(i) - x_cv(i-1);
            %           s_s = x_cv(i) - x_cv(i-1);

            a_W(i,j) = 0;
            a_S(i,j) = k(i,j)*W/d_PS;
```

```
        a_E(i,j) = 0;
        a_N(i,j) = 0;
        a_P(i,j) = a_W(i,j)+a_S(i,j)+a_E(i,j)+a_N(i,j)+ alpha;
        b_P(i,j) = alpha*T_amb;

    elseif j == 1
        d_PN = y_p(j+1) - y_p(j);

        %           s_e = y_cv(j) - y_cv(j-1);
        %           s_w = y_cv(j) - y_cv(j-1);
        %           s_n = x_cv(i) - x_cv(i-1);
        %           s_s = x_cv(i) - x_cv(i-1);

        a_W(i,j) = 0;
        a_S(i,j) = 0;
        a_E(i,j) = 0;
        a_N(i,j) = k(i,j)*W/d_PN;
        a_P(i,j) = a_W(i,j)+a_S(i,j)+a_E(i,j)+a_N(i,j)+ alpha_s;
        b_P(i,j) = alpha_s*T_amb;
    elseif i == 1
        d_PE = x_p(i+1) - x_p(i);

        a_W(i,j) = 0;
        a_S(i,j) = 0;
        a_E(i,j) = k(i,j)*W/d_PE;
        a_N(i,j) = 0;
        a_P(i,j) = a_W(i,j)+a_S(i,j)+a_E(i,j)+a_N(i,j)+ alpha_s;
        b_P(i,j) = alpha_s*T_amb;

    elseif i == N+2
        d_PW = x_p(i) - x_p(i-1);

        a_W(i,j) = k(i,j)*W/d_PW;
        a_S(i,j) = 0;
        a_E(i,j) = 0;
        a_N(i,j) = 0;
        a_P(i,j) = a_W(i,j)+a_S(i,j)+a_E(i,j)+a_N(i,j)+ alpha_s;
        b_P(i,j) = alpha_s*T_amb;
    else
        d_PE = x_p(i+1) - x_p(i);
        d_PW = x_p(i) - x_p(i-1);
        d_PN = y_p(j+1) - y_p(j);
        d_PS = y_p(j) - y_p(j-1);

        s_e = y_cv(j) - y_cv(j-1);
        s_w = y_cv(j) - y_cv(j-1);
        s_n = x_cv(i) - x_cv(i-1);
        s_s = x_cv(i) - x_cv(i-1);

        % equivalent conductivity

        d_Pe = x_cv(i) - x_p(i);
        d_Ee = x_p(i+1) - x_cv(i);
```

```
            d_Pw = x_p(i) - x_cv(i-1);
            d_Ww = x_cv(i-1) - x_p(i-1);

            d_Pn = y_cv(j) - y_p(j);
            d_Nn = y_p(j+1) - y_cv(j);

            d_Ps = y_p(j) - y_cv(j-1);
            d_Ss = y_cv(j-1) - y_p(j-1);

            k_e(i,j) = 1/(d_Pe/k(i,j) + d_Ee/k(i+1,j));
            k_w(i,j) = 1/(d_Pw/k(i,j) + d_Ww/k(i-1,j));
            k_n(i,j) = 1/(d_Pn/k(i,j) + d_Nn/k(i,j+1));
            k_s(i,j) = 1/(d_Ps/k(i,j) + d_Ss/k(i,j-1));

            a_W(i,j) = k_w(i,j)*s_w*W;
            a_S(i,j) = k_s(i,j)*s_s*W;
            a_E(i,j) = k_e(i,j)*s_e*W;
            a_N(i,j) = k_n(i,j)*s_n*W;
            a_P(i,j) =
a_W(i,j)+a_S(i,j)+a_E(i,j)+a_N(i,j)+rho(i,j)*cp(i,j)*V(i,j)/dt;

        end

    end
end

% Top nodes (natural convection)
counter = 1;
T_wire = ones(1,final_time/dt)*T_initial;
T_stator = ones(1,final_time/dt)*T_initial;
for t = dt:dt:final_time
    counter = counter +1;
    T_old = T;
    error = 1;
    T_prev = T;
    while error > delta

        for i=1:N+2
            for j = 1:M+2

                if i>1 && j>1 && i<N+2 && j<M+2
                    b_P(i,j) = qv(i,j)*V(i,j) +
rho(i,j)*cp(i,j)*V(i,j)*T_old(i,j)/dt;
                    T(i,j) = (a_E(i,j)*T(i+1,j) + a_W(i,j)*T(i-1,j) +
a_N(i,j)*T(i,j+1) + a_S(i,j)*T(i,j-1)+b_P(i,j))/a_P(i,j);
                end

                if i==1 && j~=1 && j~=M+2
                    T(i,j) = (a_E(i,j)*T(i+1,j)+b_P(i,j))/a_P(i,j);
                end

                if i==N+2 && j~=1 && j~=M+2
                    T(i,j) = (a_W(i,j)*T(i-1,j)+b_P(i,j))/a_P(i,j);
                end
```

```
                if j==1 && i~=1 && i~=N+2
                    T(i,j) = (a_N(i,j)*T(i,j+1)+b_P(i,j))/a_P(i,j);
%                     T(i,j) = T(i,j+1);
                end

                if j==M+2 && i~=1 && i~=N+2
                    T(i,j) = (a_S(i,j)*T(i,j-1)+b_P(i,j))/a_P(i,j);
                end
                T(1,M+2) = T(1,M+1);
                T(N+2,M+2) = T(N+2,M+1);
                T(1,1) = T(1,2);
                T(N+2,1) = T(N+2,2);
            end
        end
        error = max(max(abs(T-T_prev)));
        T_prev = T_prev + fr*( T - T_prev);
    end
    % plot

    if mod(t,1000)==0

        figure(1)
        contourf(X',Y',T,'ShowText','on')
        title('Temperature contour in the motorette (degree C)')
        xlabel('x axis length of bar (m)')
        ylabel('y axis length of bar (m)')
        colorbar
        grid on
        pause(1)
    end
    T_wire (counter) = T(round(N/2),4);
    T_stator (counter) = T(round(N/2),M+2);
end

%% plot

figure(2)
contourf(X',Y',T,'ShowText','on')
title('Temperature contour in the motorette (degree C)')
xlabel('x axis length of bar (m)')
ylabel('y axis length of bar (m)')
colorbar
grid on
time = 0:dt:final_time;
time = time./3600;
figure(3)
plot(time,T_wire,time,T_stator)
grid on
```